

Reply to Anonymous Referee #1

In the following, the referee's comments are reproduced (black) along with our replies (blue) and changes made to the text (red) in the revised manuscript.

Dewald et al. present measurement of NO_3 reactivity (k^{NO_3}) resulting from the reaction of NO_3 with isoprene and stable trace gases in an atmospheric simulation chamber with different initial conditions. The agreement between $\sum k_i[\text{VOC}]_i$ and k^{NO_3} indicates that NO_3 reactivity is dominated by the reaction between NO_3 and isoprene. Box model simulation results indicate that the discrepancy between measured k^{NO_3} and non-steady-state reactivity $k_{\text{NSS}}^{\text{NO}_3}$ is caused by the uncertainty in $k_{\text{RO}_2+\text{NO}_3}$.

Instrument analysis is adequate. However the authors should expand the description of instrument calibration for PTR-TOF-MS (see minor comments below).

Overall, this study reports high quality data obtained from well designed experiments. The data should be of interest to the atmospheric science community. This manuscript is well within the scope of ACP. I recommend that the manuscript be published in ACP after minor revision.

We thank the referee for the positive evaluation of our manuscript and the useful comments.

1. Minor comments

2.3 VOC measurements: PTR-ToF-MS: Please describe how often were the instruments calibrated during the campaign.

Calibration of PTR1000 was done once per day (around 5 p.m.) following the procedure as described in Holzinger et al. (2019) and took around 10 min. VOCUS PTR performed calibrations on an hourly basis for 5 minutes. This information has been integrated into the manuscript:

L151: Data processing was done using PTRwid (Holzinger, 2015) and the quantification/calibration was done once per day following the procedure as described recently (Holzinger et al., 2019).

L154: Calibration was performed on an hourly basis for 5 minutes.

Please show the variability of the instrumental sensitivities during the entire campaign period.

The sensitivity mostly varies with the primary ion signal as long as other conditions are kept constant (not the case for the whole campaign). The authors therefore do not see the benefit of providing this information in scope of this analysis.

Please be more specific about the uncertainty used in instrument comparison. It would be useful to add a figure showing the VOCs mixing ratios measured by the two PTR-TOF-MS from the same air sample.

The uncertainty associated with the isoprene measurement is 14 %. A new figure (S1) showing the isoprene mixing ratios measured by the two PTR-ToF-MS during two exemplary experiments has been added to the supplement and is mentioned in the manuscript (L155):

The isoprene measurements of the two instruments agreed mostly within the uncertainties (14 %). An exemplary comparison between the two instruments of an isoprene measurement can be found in the supplement (Fig. S1).

2.5 Box model: "FACSIMILE/CHEKMAT" is a dated tool. A quick search of it didn't return much useful information. It would be great if the simulations in this study were run in an open source, modern box model, such as BOXMOX (Knote et al., 2015), FOAM (Wolfe et al., 2016), and CAABA (Sander et al.,

2019). Doing so enables the reader to run the simulation on their own computer and play around with the configurations, such as the reaction rate constant $k_{RO_2+NO_3}$, the wall loss rates of NO_3 etc.

We present the full chemical scheme used in the simulations. Anyone who wants to reproduce or check our simulations has all the necessary information and can make their own choice of numerical integration tool.

Page 8, Line 227: “no propene data was available”: is this due to the unavailability of propene in the standard gas? If so, the expected sensitivity of propene can be calculated using the method described in Holzinger et al. (2019). The uncertainty of propene mixing ratios introduced from using expected sensitivity should be smaller than using model estimation. Please justify why the propene mixing ratios were assessed with the model instead of calculated using its sensitivity.

The reviewer is right that, in principle, propene VMR could be assessed from basic reaction kinetics according to Holzinger et al. (2019). However, the $C_3H_6H^+$ ion is also a prominent fragment originating from several compounds (e.g. isoprene) and therefore we used modelled concentrations. In addition, propene was not detectable by the VOCUS PTR as a low mass filter was used.

Page 8, Line 242: Please provide output from the unweighted linear regression (e.g., correlation coefficient, p-value), and incorporate the output into your discussion on the agreement between $\sum k_i[VOC]_i$ and k^{NO_3} measurements.

Done. We provided the correlation coefficient r of 0.95 (also denoted in Figure 2(b)) and now write (L245): A correlation coefficient of 0.95 underlines linearity of the whole data set despite increased scatter caused by the unfavourable conditions during type 2 experiments.

Page 13, Line 388–395: Please merge the model output (with $k_{wall} = 0 \text{ s}^{-1}$) in Figure S3 to Figure 9, this could help the reader better visualize the effect of introducing the NO_3 and N_2O_5 wall loss.

Done. Figure 9 has been changed accordingly. In order to preserve legibility of the NO_3 and N_2O_5 measurements after implementation of the model output in (old) Fig. S3 to Fig. 9 the order and sizes of the panels were changed. Old Fig. S3 has been removed. The caption of Fig. 9 now reads:

Figure 9: O_3 , NO_2 , NO_3 , N_2O_5 and isoprene mixing ratios and NO_3 reactivity on 2nd August (black). The grey shaded area symbolizes the overall uncertainty associated with each measurement. Orange circles denote the reactivity obtained using Eq.(3). The results of the numerical simulation using MCM v.3.3.1 with NO_3 and N_2O_5 wall loss rates set to 0 s^{-1} (model 1) are shown by black lines. The model output with introduction of NO_3 and N_2O_5 wall loss rates of 0.016 s^{-1} and $3.3 \times 10^{-4} \text{ s}^{-1}$ respectively for each of the reactants is shown by a red line (model 2), whereas the blue line (model 3) shows the result of model 2 with the rate coefficient for reaction between NO_3 and RO_2 set to $4.6 \times 10^{-12} \text{ cm}^3 \text{ molecule}^{-1} \text{ s}^{-1}$, which is twice the value estimated by the MCM.

Please discuss more about the effect of omitting the NO_3 and N_2O_5 wall loss and its cause of large discrepancies between the measurement and model simulation in NO_3 , N_2O_5 , and isoprene mixing ratios.

The changes in Figure 9 and this comment necessitated to following changes in the manuscript text (L396-410):

We examined the effect of introducing the NO_3 and N_2O_5 wall loss rate constants calculated as described above into the chemical scheme used in the box model (~~Model 1~~, MCM v3.3.1). The results from three different model outputs for the experiment on the 2nd August are summarised in Fig. 9 which compares simulated and measured mixing ratios of NO_3 , N_2O_5 , NO_2 , O_3 and isoprene (following its addition at 11:00) as well as the measured and non-steady-state NO_3 reactivities k^{NO_3} and $k_{nss}^{NO_3}$. The omission of NO_3/N_2O_5 wall losses (Model 1) results in simulated NO_3 and N_2O_5 mixing ratios up to 1400

and 1600 pptv during the isoprene-free period, which exceed measurements by factors of 4-8. This is because the only loss process for these species in this phase is the dilution rate that is two orders of magnitude lower than the estimated wall loss rates. Such high amounts of $\text{NO}_3/\text{N}_2\text{O}_5$ in the ppbv range result in rapid depletion of nearly half of the total injected isoprene within the first minute which is why Model 1 cannot describe the measurements either before or after the injection. Model 2 (red lines) includes the estimated wall loss rates and reproduces the measurements more accurately: The NO_2 and O_3 mixing ratios are accurately simulated. Furthermore, NO_3 and N_2O_5 mixing ratios that are only 10 to 30% higher than those measured and therefore NO_3 reactivities lower than $k_{\text{NSS}}^{\text{NO}_3}$ (orange circles) are predicted. ~~We note that, in these isoprene-free phases, the omission of wall losses results in model predictions of NO_3 and N_2O_5 mixing ratios up to 1400 and 1600 pptv, which exceed measurements by factors of 4-8, as illustrated in (Fig. S3).~~

Please discuss how is the first-order wall loss rate for O_3 , H_2O_2 , HO, HONO and HNO_3 derived in Table S1.

The wall loss rates were derived as previously described (Richter, 2007). Compared to losses by dilution and reactions, this is a very minor sink that does not have a significant impact on the fate of NO_3 .

The appropriate reference was added to table S1.

Page 13, Line 391: “and isoprene (following its addition at 10:50)”: from Figure 9 and Figure S2, NO_2 appeared to be injected at 10:50, isoprene appeared to be injected at 11:00, please clarify.

Correct. NO_2 was injected at 10:50 and isoprene at 11:00 UTC.

We corrected this in the manuscript.

Page 22, Figure 2(b): To better aid visual inspection of the dataset, please set the aspect ratio of x:y to 1:1, add grid to x-axis and y-axis, add border to the legend (not shown in the demo below). See Figure 2(b).

Done. Figure 2(b) has been changed accordingly.

2. Additional changes

L423: Optimum agreement irrespective of uncertainties would be achieved with a value of $9.2 \times 10^{-12} \text{ cm}^3 \text{ molecule}^{-1} \text{ s}^{-1}$ for $k_{\text{RO}_2+\text{NO}_3}$ (i.e. a factor of 4 higher than in MCM) which is demonstrated in a comparable experiment under dry conditions on the 10th August (see Fig. S4 in the supplement).

L443,483: “within uncertainties” added

Caption Fig. S4: The results of the numerical simulation using MCM v.3.3.1 (with NO_3 and N_2O_5 wall loss rate of 0.016 s^{-1} and $3.3 \times 10^{-4} \text{ s}^{-1}$ respectively) for each of the reactants is shown by a red line, whereas the blue line shows the result of the same model with ~~a doubled reaction constant for NO_3 + RO_2 reactions ($k_{\text{NO}_3+\text{RO}_2} = 9.2 \times 10^{-12} \text{ cm}^3 \text{ molecule}^{-1} \text{ s}^{-1}$)~~

3. References

Richter, C.A.: Ozone Production in the Atmosphere Simulation Chamber SAPHIR, Ph.D. thesis, Forschungszentrum Jülich GmbH, University of Köln, http://user.fz-juelich.de/record/62596/files/Energie&Umwelt_02.pdf, 2007. (pp 37, 123)

Holzinger, R., Acton, W. J. F., Bloss, W. J., Breitenlechner, M., Crilley, L. R., Dusanter, S., Gonin, M., Gros, V., Keutsch, F. N., Kiendler-Scharr, A., Kramer, L. J., Krechmer, J. E., Languille, B., Locoge, N., Lopez-Hilfiker, F., Materić, D., Moreno, S., Nemitz, E., Quéléver, L. L. J., Sarda Esteve, R., Sauvage, S., Schallhart, S., Sommariva, R., Tillmann, R., Wedel, S., Worton, D. R., Xu, K., and Zaytsev, A.: Validity and limitations of simple reaction kinetics to calculate concentrations of organic compounds from ion counts in PTR-MS, Atmos. Meas. Tech., 12, 6193–6208, <https://doi.org/10.5194/amt-12-6193-2019>, 2019.

Reply to Anonymous Referee #2

In the following, the referee's comments are reproduced (black) along with our replies (blue) and changes made to the text (red) in the revised manuscript.

The authors report on studies of NO₃ reactivity during 'nighttime' experiments in the SAPHIR chamber, with a primary focus on isoprene chemistry. An FT-CRDS system is used to determine the NO₃ reactivity with respect to stable products in the chamber, while a box model analysis is used to assess additional NO₃ losses (reaction with peroxy radicals, chamber wall losses) not determined by the FT-CRDS system. Among the key findings are the following: the FT-CRDS accurately measures the NO₃ reactivity towards isoprene, and functions well under the conditions studied; stable products of the NO₃/isoprene chemistry do not contribute significantly to NO₃ reactivity; the generic (and highly uncertain) RO₂ + NO₃ rate coefficient may be a factor of two or more higher than current estimates. Overall, this is a very solid paper that certainly is publishable in ACP. The paper is well written, and assumptions and uncertainties in the measurements are generally presented in detail. A few questions and suggestions are presented below for the authors to consider.

We thank the referee for the positive evaluation of our manuscript and the useful comments.

1. Referee's comments

There are assumptions and caveats associated with equation (1), line 220 – Could there be significant reaction products that the PTR-MS is unable to detect? Could some products not make it into the flow tube for detection by the k(NO₃) instrument? NO₃ losses due to chamber walls and radicals are not measured by the k(NO₃) instrument. Most (or maybe all) of these are dealt with at different points in the manuscript, but a clear statement or two delineating these at this point might be helpful to the reader.

This is indeed necessary for validity of Eq. (1). We now write (L219):

The VOC contribution to the NO₃ reactivity is the summed, first-order loss rate coefficient attributed to all non-radical VOCs present in the chamber that can be transported to the FT-CRDS according to Eq. (1):

Can the authors be more quantitative regarding the β-caryophyllene expt (Fig 3a)? -e.g., What is its expected lifetime? The k(NO₃) instrument is clearly not seeing the full impact of the stated addition of 2 ppbv β-caryophyllene.

Assuming 120 ppbv of O₃ and a rate constant of $1.2 \times 10^{-14} \text{ cm}^3 \text{ molecule}^{-1} \text{ s}^{-1}$ (298 K, IUAPC) for the reaction between β-caryophyllene and O₃ leads to a loss rate of 0.035 s^{-1} . Neglecting secondary oxidation, only 11 pptv of β-caryophyllene (resulting in k^{NO_3} of 0.005 s^{-1} , which is the setup's LOD) are left after 150 s. The instrument was zeroing until a couple of minutes after the injection of β-caryophyllene and thus detected only the last residues of this sticky monoterpene. We add this point to the manuscript and now write (L258):

The instrument was zeroing until shortly after the injection of this terpene. ~~The presence of β-caryophyllene explains the small increase in the NO₃ reactivity after 08:30 UTC. As the lifetime of β-caryophyllene is extremely short in the chamber under the given conditions (~ 150 s), only the small fraction of unreacted β-caryophyllene contribute to the k^{NO_3} signal observed after 08:40 UTC.~~

Line 265 / Fig 3b: Isoprene loss here is due to reaction with O₃, I assume (maybe also OH formed in the ozonolysis)? Does the agreement noted between the k(NO₃) instrument and the k[isoprene] calculation imply that major isoprene ozonolysis products are also comparatively unreactive towards NO₃? (Also, a minor detail, but the isoprene decay seems more rapid than would be implied by the O₃ concentration given?)

Correct, the isoprene loss is mainly caused by ozonolysis but also by dilution during the first three hours between 06:50 and 09:50 UTC. Using stated initial concentrations and rate coefficients at 298 K (IUPAC, 2019) calculated losses are as follows:

$$k_{loss}(isoprene) = k_{ozonolysis} + k_{dilution} = [O_3] * k_{O_3+isoprene} + k_{dilution} \\ = (3.11 * 10^{-5} + 1.5 * 10^{-5}) s^{-1} = 4.61 * 10^{-5} s^{-1}$$

$$[isoprene](3 h) \approx [Isoprene]_0 * \exp(-k_{loss}(isoprene) * 10800 s) \\ \approx 4 ppbv * \exp(-4.61 * 10^{-5} s^{-1} * 10800 s) \approx 2.4 ppbv$$

After 3 hours 2.4 ppbv of isoprene causing an NO₃ reactivity of 0.038 s⁻¹ which is in good agreement with the measurement. The sudden decrease in isoprene (and k^{NO_3}) after 09:50 UTC is caused by an increase of the dilution flow by a factor of 10 in scope of a humidification process.

We agree, the good agreement between the FT-CRDS measurement and k[isoprene] suggests a neglectable contribution of products from the ozonolysis. Given the low reactivity of stable ozonolysis products (e.g. MACR, MVK, formaldehyde) and the non-detection of radicals/Criegee intermediates this seems to be a valid conclusion. We include these aspects to the manuscript (L267):

Isoprene depletion is dominated by ozonolysis at this phase, whereas the sudden drop in k^{NO_3} is caused by an increased dilution flow during humidification of the chamber around 10:00 UTC. The absence of NO₂ results in a more accurate, less scattered measurement of k^{NO_3} and underscores the reliability of the measurement under favourable conditions. All of the observed reactivity can be assigned to isoprene that was injected at 06:52 UTC. This implies that stable secondary oxidation of products from isoprene ozonolysis (such as formaldehyde, MACR, MVK) are insignificant for k^{NO_3} which is consistent with the low rate coefficients (e.g. $k_{MACR+NO_3} = 3.4 \times 10^{-15} cm^3 molecule^{-1} s^{-1}$ as highest of the three; IUPAC, 2019).

Line 312 or so - It should be noted here that NC4CHO is only one of many products that can be formed. Correction made, we now write (L319):

One of several ~~the~~ major, stable oxidation products according to MCM is an organic nitrate with aldehyde functionality (O₂NOC₄H₆CHO, NC4CHO).

In Figure 9, it is not clear to me that the increased RO₂ + NO₃ rate coefficient improves the model/measured NO₃ comparison?

This statement referred to the very first phase after the isoprene injection, but we agree that in the last phase of the experiment (old) model 2 shows a worse agreement with the NO₃ measurement than (old) model 1. We now write (L419):

The higher rate coefficient for reaction of NO₃ with RO₂ would be sufficient to ~~not only~~ explain the observed discrepancy between the overall reactivity $k_{nss}^{NO_3}$ and k^{NO_3} within the uncertainties associated with the analysis. ~~but also results in a better reproduction of the NO₃ measurement during the isoprene-dominated period.~~

2. Additional changes

L423: Optimum agreement irrespective of uncertainties would be achieved with a value of $9.2 \times 10^{-12} \text{ cm}^3 \text{ molecule}^{-1} \text{ s}^{-1}$ for $k_{\text{RO}_2+\text{NO}_3}$ (i.e. a factor of 4 higher than in MCM) which is demonstrated in a comparable experiment under dry conditions on the 10th August (see Fig. S4 in the supplement).

L443,483: “within uncertainties” added

Caption Fig. S4: The results of the numerical simulation using MCM v.3.3.1 (with NO_3 and N_2O_5 wall loss rate of 0.016 s^{-1} and $3.3 \times 10^{-4} \text{ s}^{-1}$ respectively) for each of the reactants is shown by a red line, whereas the blue line shows the result of the same model with ~~a doubled reaction constant for NO_3 + RO_2 reactions~~ ($k_{\text{NO}_3+\text{RO}_2} = 9.2 \times 10^{-12} \text{ cm}^3 \text{ molecule}^{-1} \text{ s}^{-1}$).

3. References

IUPAC: Task Group on Atmospheric Chemical Kinetic Data Evaluation, (Ammann, M., Cox, R.A., Crowley, J.N., Herrmann, H., Jenkin, M.E., McNeill, V.F., Mellouki, A., Rossi, M. J., Troe, J. and Wallington, T. J.) <http://iupac.pole-ether.fr/index.html>, 2019.

Evolution of NO₃ reactivity during the oxidation of isoprene

Patrick Dewald¹, Jonathan M. Liebmann¹, Nils Friedrich¹, Justin Shenolikar¹, Jan Schuladen¹, Franz Rohrer², David Reimer², Ralf Tillmann², Anna Novelli², Changmin Cho², Kangming Xu³, Rupert Holzinger³, François Bernard^{4,a}, Li Zhou⁴, Wahid Mellouki⁴, Steven S. Brown^{5,6}, Hendrik Fuchs², Jos Lelieveld¹ and John N. Crowley¹

¹Atmospheric Chemistry Department, Max Planck Institut für Chemie, 55128 Mainz, Germany

²Institute of Energy and Climate Research, IEK-8: Troposphere, Forschungszentrum Jülich GmbH, 52428 Jülich, Germany

³Institute for Marine and Atmospheric Research, IMAU, Utrecht University, Utrecht, Netherlands

⁴Institut de Combustion, Aérothermique, Réactivité et Environnement (ICARE), CNRS (UPR 3021) /OSUC, 1C Avenue de la Recherche Scientifique, 45071 Orléans Cedex 2, France

⁵NOAA Chemical Sciences Laboratory, 325 Broadway, Boulder, CO 80305, USA

⁶Department of Chemistry, University of Colorado, Boulder, CO 80209, USA

^anow at: Laboratoire de Physique et Chimie de l'Environnement et de l'Espace (LPC2E), Centre National de la Recherche Scientifique (CNRS), Université d'Orléans, Observatoire des Sciences de l'Univers en région Centre - Val de Loire (OSUC), Orléans, France

Correspondence to: John N. Crowley (john.crowley@mpic.de)

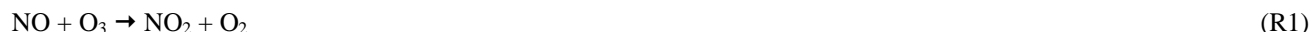
Abstract. In a series of experiments in an atmospheric simulation chamber (SAPHIR, Forschungszentrum Jülich, Germany) NO₃ reactivity (k^{NO_3}) resulting from the reaction of NO₃ with isoprene and stable trace gases formed as products was measured directly using a flow-tube reactor coupled to a cavity-ring-down spectrometer (FT-CRDS). The experiments were carried out in both dry and humid air with variation of the initial mixing ratios of ozone (50 – 100 ppbv), isoprene (3 – 22 ppbv) and NO₂ (5 – 30 ppbv). k^{NO_3} was in excellent agreement with values calculated from the isoprene mixing ratio and the rate coefficient for the reaction of NO₃ with isoprene. This result serves both to confirm that the FT-CRDS returns accurate values of k^{NO_3} even at elevated NO₂ concentrations and to show that reactions of NO₃ with stable reaction products like non-radical organic nitrates do not contribute significantly to NO₃ reactivity during the oxidation of isoprene. A comparison of k^{NO_3} with NO₃ reactivities calculated from NO₃ mixing ratios and NO₃ production rates suggests that organic peroxy radicals and HO₂ account for ~ 50% of NO₃ losses. This contradicts predictions based on numerical simulations using the Master Chemical Mechanism (MCM version 3.3.1) unless the rate coefficient for reaction between NO₃ and isoprene-derived RO₂ is roughly doubled to $\approx 5 \times 10^{-12} \text{ cm}^3 \text{ molecule}^{-1} \text{ s}^{-1}$.

1 Introduction

The atmospheric oxidation of volatile organic compounds (VOCs) of both biogenic and anthropogenic origin has a great impact on tropospheric chemistry and global climate (Lelieveld et al., 2008). Isoprene is one of the major organic (non-methane) compounds that is released in the environment by vegetation and contributes ~ 50% to the overall emission of VOCs into the atmosphere (Guenther et al., 2012). The most important initiators of oxidation for biogenic VOCs in the atmosphere are

hydroxyl radicals (OH), ozone (O₃) and nitrate radicals (NO₃) (Geyer et al., 2001; Atkinson and Arey, 2003; Lelieveld et al., 2016; Wennberg et al., 2018). Our focus in this study is on NO₃, which is formed via the sequential oxidation of NO by ozone (R1 and R2). During the daytime, NO₃ mixing ratios are very low owing to its efficient reaction with NO (R6) and its rapid photolysis (R7 and R8). Generally, NO₃ is present in mixing ratios greater than a few pptv only at night-time, when it can become the major oxidizing agent for VOCs including isoprene (R5). In forested regions, reactions with biogenic trace gases can however contribute significantly to the daytime reactivity of NO₃ (Liebmann et al., 2018a; Liebmann et al., 2018b).

Moreover, NO₂, NO₃ and N₂O₅ exist in thermal equilibrium (R3 and R4) so that the heterogeneous loss of N₂O₅ (and NO₃) at surfaces (R9 and R10) impacts on the lifetime of NO₃ in the atmosphere (Martinez et al., 2000; Brown et al., 2003; Brown et al., 2006; Brown et al., 2009b; Crowley et al., 2010).



Although isoprene is mainly emitted by vegetation at daytime (Sharkey and Yeh, 2001; Guenther et al., 2012), during which its main sink reaction is with the OH radical (Paulot et al., 2012), it accumulates in the nocturnal boundary layer (Warneke et al., 2004; Brown et al., 2009a) where reactions of NO₃ and O₃ determine its lifetime (Wayne et al., 1991; Brown and Stutz, 2012; Wennberg et al., 2018). The rate constant (at 298 K) for the reaction between isoprene and NO₃ is $6.5 \times 10^{-13} \text{ cm}^3 \text{ molecule}^{-1} \text{ s}^{-1}$, which is several orders of magnitude larger than for the reaction with O₃ ($1.28 \times 10^{-17} \text{ cm}^3 \text{ molecule}^{-1} \text{ s}^{-1}$) (Atkinson et al., 2006; IUPAC, 2019) thus compensating for the difference in mixing ratios of NO₃ (typically 1-100 pptv) and O₃ (typically 20-80 ppbv) (Edwards et al., 2017). NO₃ is often the most important nocturnal oxidant of biogenic VOCs (Mogensen et al., 2015) especially in remote, forested environments where it reacts almost exclusively with biogenic isoprene and terpenes (Ng et al., 2017; Liebmann et al., 2018a; Liebmann et al., 2018b). The reaction between isoprene and NO₃ leads initially to the formation of nitro isoprene peroxy radicals (NISOPPOO, e.g. O₂NOCH₂C(CH₃)=CHCH₂OO) that can either react with NO₃ forming mostly a nitro isoprene aldehyde (NC4CHO, e.g. O₂NOCH₂C(CH₃)=CHCHO) and methyl vinyl ketone (MVK) or react further with other organic peroxy (RO₂) or hydroperoxy (HO₂) radicals forming nitrated carbonyls, peroxides and alcohols (Schwantes et al., 2015).

The organic nitrates formed (RONO_2) can deposit on particles (R11) and therefore the NO_3 + isoprene system contributes to the formation of secondary organic aerosols (SOA) (Rollins et al., 2009; Fry et al., 2018). Together with heterogeneous uptake of N_2O_5 or NO_3 on particle surfaces (R9 and R10), the build-up of SOA from isoprene oxidation products forms a significant pathway for removal of reactive nitrogen species (NO_x) from the gas phase; a detailed understanding of the reaction between isoprene and NO_3 is therefore crucial for assessing its impact on SOA formation and NO_x lifetimes.

In this study, the NO_3 -induced oxidation of isoprene was examined in an environmental chamber equipped with a large suite of instruments including a cavity-ring-down spectrometer coupled to a flow-tube reactor (FT-CRDS) for direct NO_3 reactivity measurement (Liebmann et al., 2017). The NO_3 lifetime in steady-state (the inverse of its overall reactivity) has often been derived from NO_3 mixing ratios and production rates, the latter depending on the mixing ratios of NO_2 and O_3 (Heintz et al., 1996; Geyer and Platt, 2002; Brown et al., 2004; Sobanski et al., 2016b). The steady-state approach works only if NO_3 is present at sufficiently large mixing ratios to be measured (generally not the case during daytime), breaks down to a varying extent if steady state is not achieved (Brown et al., 2003; Sobanski et al., 2016b) and may be influenced by heterogeneous losses of NO_3 or N_2O_5 (Crowley et al., 2011; Phillips et al., 2016) which are difficult to constrain. Comparing the steady-state calculations with the FT-CRDS approach (which derives the NO_3 reactivity attributable exclusively to VOCs) can provide insight into the main contributions to NO_3 reactivity and its evolution as the reaction progresses. In the following, we present the results of direct NO_3 reactivity measurements in the SAPHIR environmental chamber under controlled conditions and explore the contributions of isoprene, peroxy radicals and stable oxidation products to NO_3 reactivity over a period of several hours as the chemical system resulting from NO_3 induced oxidation of isoprene evolves.

2 Measurement and instrumentation

An intensive study of the NO_3 + isoprene system (NO3ISOP campaign) took place at the SAPHIR chamber of the Forschungszentrum Jülich over a three-week period in August 2018. The aim of NO3ISOP was to improve our understanding of product formation in the reaction between NO_3 and isoprene as well as its impact on the formation of secondary organic aerosols (SOA). Depending on the conditions (high or low HO_2/RO_2 , temperature, humidity, daytime or night-time) a large variety of oxidation products, formed via different reaction paths exist (Wennberg et al., 2018). During NO3ISOP, the impact of varying experimental conditions on the formation of gas phase products as well as secondary organic aerosol formation and composition was explored within 22 different experiments (see Table 1). Typical conditions were close to those found in the atmosphere with 5 ppbv of NO_2 , 50-100 ppbv of O_3 and 3 ppbv of isoprene or (when high product formation rates were required) the NO_2 was raised to 25 ppbv and isoprene to 10 ppbv. The high O_3 mixing ratios in the chamber ensured that NO was not detectable (< 10 pptv) in the darkened chamber.

The first 11 experiments of the NO3ISOP were dedicated to gas-phase chemistry; in the second part seed-aerosol ($(\text{NH}_4)_2\text{SO}_4$) was added and the focus shifted to aerosol measurements. Due to a contamination event in the chamber the experiment from

the 7th August is not considered for further analysis. The SAPHIR chamber and the measurements/instruments that are relevant for the present analysis are described briefly below.

100 2.1 The SAPHIR chamber

The atmospheric simulation chamber SAPHIR has been described in detail on various occasions (Rohrer et al., 2005; Bossmeyer et al., 2006; Fuchs et al., 2010) and we present only a brief description of some important features here: The outdoor chamber consists of two layers of FEP foil defining a cylindrical shape with a volume of 270 m³ and a surface area of 320 m². The chamber is operated at ambient temperature and its pressure is ~30 Pa above ambient level. A shutter system in the roof
105 enables the chamber to be completely darkened or illuminated with natural sunlight. Two fans result in rapid (2 min) mixing of the gases in the chamber, which was flushed with 250 m³ h⁻¹ of synthetic air (obtained from mixing high purity nitrogen and oxygen) for several hours between each experiment. Leakages and air consumption by instruments leads to a dilution rate of typically 1.4 x 10⁻⁵ s⁻¹. Coupling to a separate plant chamber enabled the introduction of plant emissions into the main chamber (Hohaus et al., 2016).

110 2.2 NO₃ reactivity measurements: FT-CRDS

The FT-CRDS instrument for directly measuring NO₃ reactivity (k^{NO_3}) has been described in detail (Liebmann et al., 2017) and only a brief summary is given here. NO₃ radicals are generated in sequential oxidation of NO with O₃ (reactions R1 and R2) in a darkened, thermostated glass reactor at a pressure of 1.3 bar. The reactor surfaces are coated with Teflon (DuPont, FEPD 121) to reduce the loss of NO₃ and N₂O₅ at the surface during the ~ 5 min residence time. The gas mixture exiting the
115 reactor (400 sccm) is heated to 140°C before being mixed with either zero-air or ambient air (at room temperature) and entering the FEP-coated flow-tube where further NO₃ production (R2), equilibrium reaction with N₂O₅ (R3 and R4) as well as NO₃ loss via reactions with VOCs/NO (R5/R6) or with the reactor wall (R10) take place. NO₃ surviving the flow reactor after a residence time of 10.5 s is quantified by CRDS at a wavelength of 662 nm. The NO₃ reactivity is calculated from relative change in NO₃ concentration when mixed with zero-air or ambient air. In order to remove a potential bias by ambient NO₃/N₂O₅, sampled air
120 is passed through an uncoated 2L glass flask (~60 s residence time) heated to 45°C to favour N₂O₅ decomposition before reaching the flowtube. Ambient NO₃ (or other radicals, e.g. RO₂) is lost by its reaction with the glass walls. In addition to the reaction of interest (R5), reactions (R2) to (R4) and (R10) affect the measured NO₃ concentration so that corrections via numerical simulation of this set of reactions are necessary to extract k^{NO_3} from the measured change in NO₃ concentration, necessitating accurate measurement of O₃, NO and especially NO₂ mixing ratios. For this reason, the experimental setup was
125 equipped with a second cavity for the measurement of NO₂ at 405 nm as described recently (Liebmann et al., 2018b). In its current state the instrument's detection limit is ~ 0.005 s⁻¹. By diluting highly reactive ambient air with synthetic air, ambient reactivities up to 45 s⁻¹ can be measured. The overall uncertainty in k^{NO_3} results from instability of the NO₃ source and the CRDS detection of NO₃ and NO₂ as well as uncertainty introduced by the numerical simulations. Under laboratory conditions, measurement errors result in an uncertainty of 16%. The uncertainty associated with the numerical simulation was estimated

130 by Liebmann et al. (2017) who used evaluated rate coefficients and associated uncertainties (IUPAC) to show that the uncertainty in k^{NO_3} is highly dependent on the ratio between the NO_2 mixing ratio and the measured reactivity. If a reactivity of 0.046 s^{-1} (e.g. from 3 ppbv of isoprene), is measured at 5 ppbv of NO_2 (typical for this campaign), the correction derived from the simulation would contribute an uncertainty of 32% to the resulting overall uncertainty of 36%. For an experiment with 25 ppbv of NO_2 and 10 ppbv of isoprene, large uncertainties ($> 100\%$) are associated with the correction procedure as the
135 NO_3 loss caused by reaction with NO_2 exceeds VOC-induced losses. Later we show that data obtained even under unfavorable conditions (high NO_2 mixing ratios) are in accord with isoprene measurements, which suggests that the recommended uncertainties in rate coefficients for R3 and R4 are overly conservative.

The sampled air was typically mixed with ~ 50 pptv of NO_3 radicals and the reaction between NO_3 and RO_2 radicals generated in the flow-tube (R5) represents a potential bias to the measurement of k^{NO_3} . In a typical experiment (e.g. 3 ppbv of isoprene)
140 the reactivity of NO_3 towards isoprene is 0.046 s^{-1} . A simple calculation shows that a total of 20 pptv of RO_2 radicals have been formed after 10.5 s reaction between NO_3 and isoprene time in the flow tube. Assuming a rate coefficient of $\sim 5 \times 10^{-12}\text{ cm}^3\text{ molecule}^{-1}\text{ s}^{-1}$ for reaction between NO_3 and RO_2 , we calculate a 5% contribution of RO_2 radicals to NO_3 loss. In reality, this value represents a very conservative upper limit as RO_2 is present at lower concentrations throughout most of the flow tube and its concentration will be significantly reduced by losses to the reactor wall and self-reaction. In our further analysis
145 we therefore do not consider this reaction.

2.3 VOC measurements: PTR-ToF-MS

During the NO3ISOP campaign, isoprene and other VOCs were measured by two different PTR-ToF-MS (Proton Transfer Reaction Time-Of-Flight Mass Spectrometer) instruments. The PTR-TOF1000 (IONICON Analytic GmbH) has a mass resolution $> 1500\text{ m}/\Delta m$ and a limit of detection $< 10\text{ ppt}$ for a 1 minute integration time. The instrumental background was
150 determined every hour by pulling the sample air through a heated tube (350°C) filled with a Pt catalyst for 10 minutes. Data processing was done using PTRwid (Holzinger, 2015) and the quantification/calibration was done **once per day** following the procedure as described recently (Holzinger et al., 2019).

The Vocus PTR (ToFwerk AG/Aerodyne Research Inc.) features a newly designed focusing ion-molecule reactor resulting in a resolving power of $12000\text{ m}/\Delta m$ (Krechmer et al., 2018). **Calibration was performed on an hourly basis for 5 minutes.** The
155 isoprene measurements of the two instruments agreed **mostly** within the uncertainties (**14 %**). **An exemplary comparison between the two instruments of an isoprene measurement can be found in the supplement (Fig. S1).** For the evaluation of the experiment on the 2nd August only data from the PTR-TOF1000 were available. For all the other experiments of the campaign, isoprene and monoterpene mixing ratios were taken from the Vocus PTR owing to its higher resolution and data coverage.

2.4 $NO_3/N_2O_5/NO_2/NO/O_3$ measurements

160 The NO_3/N_2O_5 mixing ratios used for analysis are from a harmonized data set including the measurements from two CRDS instruments. Data availability, quality and consistency with the expected $NO_3/N_2O_5/NO_2$ equilibrium ratios were criteria for

selecting which data set to use for each experiment. Both instruments measure NO₃ (and N₂O₅ after its thermal decomposition to NO₃ in a heated channel) using cavity ring down spectroscopy at a wavelength of ~662 nm. The 5-channel device operated by the Max-Planck-Institute (MPI) additionally measured NO₂ and has been described recently in detail (Sobanski et al., 2016a). Its NO₃ channel has a limit of detection (LOD) of 1.5 pptv (total uncertainty of 25%); the N₂O₅ channel has a LOD of 3.5 pptv (total uncertainty of 28% for mixing ratios between 50 and 500 pptv). Air was sub-sampled from a bypass flow drawing ~40 SLM through a 4m length of 0.5 inch (inner diameter, i.d.) PFA tubing from the chamber. Variation of the bypass flow rate was used to assess losses of NO₃ (< 10%) in transport to the instrument, for which correction was applied. Air entering the instrument was passed through a Teflon membrane filter (Pall Corp., 47mm, 0.2 µm pore) which was changed every 60 mins. Corrections for loss of NO₃ and N₂O₅ on the filter and inlet lines were carried out as described previously (Sobanski et al., 2016a).

The second CRDS was built by the NOAA Chemical Sciences Laboratory (Dubé et al., 2006; Fuchs et al., 2008; Wagner et al., 2011; Fuchs et al., 2012; Dorn et al., 2013) and was operated by the Institut de Combustion, Aérothermique, Réactivité et Environnement (ICARE). During the NO₃ISOP campaign, the NOAA-CRDS was positioned beneath the chamber and air was sampled through an individual port in the floor. The sampling flow rate was 5.5-7 L min⁻¹ through a Teflon FEP line (i.d. 1.5 mm, total length about 0.9 m) extending by about 50 cm (i.d. 4 mm) with 25 cm (i.d. 4 mm) into the chamber. A Teflon filter (25 µm thickness, 47 mm diameter, 1-2 µm pore size) was placed downstream of the inlet to remove aerosol particles, and changed automatically at an interval of 1.5 - 2 h depending on the conditions of the experiments, such as the amount of aerosol in the chamber. The instrument was operated with a noise equivalent 1σ detection limit of 0.25 and 0.9 pptv in 1s for the NO₃ and N₂O₅ channels, respectively. The total uncertainties (1σ) of the NOAA-CRDS instrument were 25% (NO₃) and -8%/+11% (N₂O₅).

NO₂ mixing ratios were taken from a harmonized data set combining the measurements of the 5-channel CRDS with that of the NO₃ reactivity setup as well as the NO_x measurement of a thermal dissociation CRDS setup (Thieser et al., 2016). The NO_x measurement could be considered as a NO₂ measurement since during dark periods of the experiments NO would have been present at extremely low levels. The total uncertainty associated with the NO₂ mixing ratios is 9%.

NO was measured with an LOD of 4 pptv via chemiluminescence (CL; (Ridley et al., 1992)) detection (ECO Physics, model TR780) and ozone was quantified with an LOD of 1 ppbv by ultraviolet absorption spectroscopy at 254 nm (Ansyco, ozone analyser 41M). Both instruments operate with an accuracy (1σ) of 5%.

2.5 Box model

The results of the chamber experiments were analysed using a box model based on the oxidation of isoprene by NO₃, OH and O₃ as incorporated in the Master Chemical Mechanism (MCM), version 3.3.1 (Saunders et al., 2003; Jenkin et al., 2015). In this work, the analysis focusses on the fate of the NO₃ radical, so that the oxidation of some minor products was omitted in order to reduce computation time. Moreover, the most recently recommended rate coefficient (IUPAC, 2019) for the reaction between NO₃ and isoprene ($k_5 = 2.95 \times 10^{-12} \exp(-450/T) \text{ cm}^3 \text{ molecule}^{-1} \text{ s}^{-1}$) was used instead of the value found in the MCM

195 v3.3.1, which is 6.8% higher. Chamber-specific parameters such as temperature, pressure as well as the time of injection and amount of trace gases added (usually O₃, NO₂ and isoprene) were the only constraints to the model. The chamber dilution flow was implemented as first-order loss rates for all trace-gases and wall loss rates for NO₃ or N₂O₅ were introduced (see Section 3.2). The numerical simulations were performed with FACSIMILE/CHEKMAT (release H010 date 28 April 1987 version 1) at 1 minute time resolution (Curtis and Sweetenham, 1987). The chemical scheme used is listed in the supplementary
200 information (Table S1).

3 Results and discussion

An overview of the experimental conditions (e.g. isoprene, NO₃, NO₂ and O₃ mixing ratios) on each day of the campaign is given in Fig. 1. The temperature in the chamber was typically between 20 and 30 °C but increased up to 40 °C when the chamber was opened to sunlight. The relative humidity was close to 0% during most of the experiments before 14th August.
205 After this date, the experiments focussed on secondary organic aerosol formation and humidified air was used.

We divide the experiments into two broad categories according to the initial conditions: Type 1 experiments were undertaken with NO₃ production from 5 ppbv of NO₂ and 100 ppbv of O₃. The addition of isoprene with mixing ratios of ~3 ppbv resulted in NO₃ reactivities of around 0.05 s⁻¹ at the time of injection. The NO₃ and N₂O₅ mixing ratios were typically of the order of several tens of pptv in the presence of isoprene under dry conditions. During humid experiments (with seed aerosol) NO₃
210 mixing ratios were mostly below the LOD in the presence of isoprene owing to increased uptake of NO₃/N₂O₅ on particles. An exceptionally large isoprene injection (~20 ppbv) resulted in the maximum NO₃ reactivity of 0.4 s⁻¹ on the 24th August. In type 2 experiments, higher NO₃ production rates were achieved by using 25 ppbv of NO₂ and 100 ppbv of O₃. In these experiments, with the goal of generating high concentrations of organic oxidation products, isoprene mixing ratios of 10 ppbv resulted in reactivities of ~0.2 s⁻¹ at the time of isoprene injection. Owing to high NO₃ production rates, several hundreds of
215 pptv of NO₃ and a few ppbv of N₂O₅ were present in the chamber.

Figure 1 shows that once isoprene has been fully removed at the end of each experiment, the NO₃ reactivity tends towards its LOD of 0.005 s⁻¹ indicating that the evolution of the NO₃ reactivity is closely linked to the changing isoprene mixing ratio.

3.1 Comparison of k^{NO_3} with calculated reactivity based on measurements of VOCs

The VOC contribution to the NO₃ reactivity is the summed, first-order loss rate coefficient attributed to all non-radical VOCs
220 present in the chamber that can be transported to the FT-CRDS according to Eq. (1):

$$k^{NO_3} = \sum k_i[VOC]_i \quad (1)$$

where k_i is the rate coefficient (cm³ molecule⁻¹ s⁻¹) for the reaction between a VOC of concentration [VOC]_{*i*} and NO₃.

Reliable values of k^{NO_3} and VOC data are available from the 2nd of August onwards (see Table 1 for experimental conditions) and were used to compare FT-CRDS measurements of k^{NO_3} with $\sum k_i[VOC]_i$. For most of the experiments, isoprene was the
225 only VOC initially present in the chamber and at the beginning of the experiments k^{NO_3} should be given by $k_5[\text{isoprene}]$, the

latter measured by the PTR-MS instruments (see above). On the 9th and 21st August, both isoprene and propene (100 ppbv) were injected into the chamber, the summed NO₃ reactivity from these trace gases was then: $k_5[\text{isoprene}] + k_{\text{propene}}[\text{propene}]$, with $k_{\text{propene}} = 9.5 \times 10^{-15} \text{ cm}^3 \text{ molecule}^{-1} \text{ s}^{-1}$ at 298 K (IUPAC, 2019). As no propene data was available, the propene mixing ratios were assessed with the model (see above) based on injected amounts as well as subsequent loss by oxidation chemistry (mainly ozonolysis) and dilution. On the 22nd August, coupling to a plant emission chamber permitted the introduction of monoterpenes and isoprene into the main chamber so that the NO₃ reactivity was $k_5[\text{isoprene}] + k_{\text{monoterpenes}}[\text{monoterpenes}]$. The uncertainty in $\Sigma k_i[\text{VOC}]_i$ was propagated from the standard deviation of the isoprene and monoterpene mixing ratios and the uncertainties of 41% in k_5 , 58% in k_{propene} (IUPAC, 2019) as well as 47% in $k_{\text{monoterpenes}}$ (average uncertainty of three dominant terpenes, see below).

Figure 2 (a) depicts an exemplary time series of k^{NO_3} and $\Sigma k_i[\text{VOC}]_i$ between the 9th and 13th of August. The measured k^{NO_3} and values of $\Sigma k_i[\text{VOC}]_i$ calculated from measured isoprene (and modelled propene in case of the 9th August) are, within experimental uncertainty, equivalent indicating that the NO₃ reactivity can be attributed entirely to its reaction with isoprene (and other reactive trace gases like propene) injected into the chamber.

The correlation between k^{NO_3} and $\Sigma k_i[\text{VOC}]_i$ for the entire campaign dataset is illustrated in Fig. 2(b). Type 2 experiments (high NO₂ mixing ratios) were included despite the unfavourable conditions for measurement of k^{NO_3} , which result in large correction factors via numerical simulation (see above). The data points obtained on the 14th August display large variability, which is likely to have been caused by non-operation of the fans leading to poor mixing in the chamber. An unweighted linear regression of the whole dataset yields a slope of 0.962 ± 0.003 indicating excellent agreement between the directly measured NO₃ and those calculated from Eq. (1). The intercept of $(0.0023 \pm 0.0004) \text{ s}^{-1}$ is below the LOD of the reactivity measurement.

A correlation coefficient of 0.95 underlines the linearity of the whole data set despite increased scatter caused by the unfavourable conditions during type 2 experiments. Note that data from the 7th August (chamber contamination) were not used. On the 15th and 21st August, additional flushing of the chamber with synthetic air (150-300 m³) and humidification shortly before the actual beginning of the experiment resulted in a constant background reactivity in k^{NO_3} of 0.04 s⁻¹ on the 15th and 0.012 s⁻¹ on the 21st August. High background reactivity was not observed during other humid experiments if the chamber was flushed extensively with synthetic air (~2000 m³) during the night between experiments and if the additional flushing was omitted. The trace gas(es) causing this background reactivity could not be identified with the available measurements, but are probably released from the chamber walls during flushing and humidification. In order to make detailed comparison with the VOC data the background reactivity, which was fairly constant, was simply added.

A more detailed examination of k^{NO_3} data from two type 1 experiments (low NO₂) is given in Fig. 3. The grey shaded areas indicate the total uncertainty associated with the FT-CRDS measurement of k^{NO_3} (Liebmann et al., 2017), the scatter in the data stems mostly from the correction procedure via numerical simulation.

On the 20th August (upper panel, Fig. 3a) in addition to NO₂ and O₃, (NH₄)₂SO₄ seed aerosol (~50 µg cm⁻³) and β-caryophyllene (~2 ppbv) were injected at 08:40 UTC in order to favour formation of secondary organic aerosol. The instrument was zeroing

until shortly after the injection of this terpene. ~~The presence of β -caryophyllene explains the small increase in the NO_3 reactivity after 08:30 UTC.~~ As the lifetime of β -caryophyllene is extremely short in the chamber under the given conditions (~ 150 s), only the small fraction of unreacted β -caryophyllene contribute to the k^{NO_3} signal observed after 08:40 UTC. At 09:20, 10:13 and 11:50 UTC isoprene was injected into the chamber resulting in step-like increases in the measured NO_3 reactivity. Each increase in reactivity and the ensuing evolution over time match well with the calculated values of $k_5[\text{isoprene}]$ (red datapoints). The red shaded area indicates the overall uncertainty in the latter. Clearly, within experimental uncertainty, the NO_3 reactivity is driven almost entirely by reaction with isoprene, with negligible contribution from stable, secondary products.

During the experiment of the 23rd August (lower panel, Fig. 3b), only isoprene and ozone were present in the chamber for the first 4 hours. Isoprene depletion is dominated by ozonolysis at this phase, whereas the sudden drop in k^{NO_3} is caused by an increased dilution flow during humidification of the chamber around 10:00 UTC. The absence of NO_2 results in a more accurate, less scattered measurement of k^{NO_3} and underscores the reliability of the measurement under favourable conditions.

All of the observed reactivity can be assigned to isoprene that was injected at 06:52 UTC. This implies that stable secondary oxidation of products from isoprene ozonolysis (such as formaldehyde, MACR, MVK) are insignificant for k^{NO_3} which is consistent with the low rate coefficients (e.g. $k_{\text{MACR}+\text{NO}_3} = 3.4 \times 10^{-15} \text{ cm}^3 \text{ molecule}^{-1} \text{ s}^{-1}$ as highest of the three; IUPAC, 2019).

The results of a type 2 experiment with NO_2 mixing ratios of ~ 20 ppbv as well as higher isoprene mixing ratios (injections of ~ 8 and ~ 3 ppbv under dry conditions) is depicted in Fig. 4 (a). Despite the requirement of large correction factors to k^{NO_3} owing to the high NO_2 to isoprene ratios, fair agreement between measured k^{NO_3} and the expected reactivity is observed for each of the isoprene injections at 07:30, 09:20 and 10:50 UTC. The agreement may indicate that the uncertainty in k^{NO_3} (grey shaded area) which is based on uncertainty in e.g. the rate coefficient for reaction between NO_3 and NO_2 (Liebmann et al., 2017) is overestimated.

In Fig. 4(b) we display the results of an experiment on 12th August, in which the initially darkened chamber (first ~ 4 hours) was opened to sunlight (final 4 hours). NO_2 mixing ratios varied between 12 and 4 ppbv and isoprene was injected (~ 3 ppbv) three times at 05:55, 07:40 and 09:45 UTC. During the dark-phase, measured k^{NO_3} follows $k_5[\text{isoprene}]$. At 11:00 UTC the chamber was opened to sunlight, during which, approximately 5 ppbv of NO_2 , 200 – 150 pptv of NO and < 1 ppbv of isoprene were present in the chamber. In this phase, the loss of NO_3 was dominated by its photolysis and reaction with NO. Within experimental uncertainty, the measured daytime k^{NO_3} after correction for both NO_2 and NO (correction factors between 0.05 and 0.02) during the sunlit period was still close to $k_5[\text{isoprene}]$.

On the 22nd August, the SAPHIR chamber was filled with air from a plant chamber (SAPHIR-PLUS) containing six European oaks (*Quercus robur*) which emit predominantly isoprene but also monoterpenes, mainly limonene, 3-carene and α -pinene (van Meeningen et al., 2016).

The time series of measured NO_3 reactivity k^{NO_3} (black datapoints) after coupling to the plant-chamber at 08:00 UTC is shown in Fig. 5. Data after 11:40 UTC is not considered as the chamber lost its pressure after several re-coupling attempts to the plant

chamber. Also plotted (red data points) is the NO_3 -reactivity calculated from $\sum k_i[\text{VOC}]_i$ whereby both isoprene and the total terpene mixing ratio (up to 500 pptv) were measured by the Vocus PTR-MS. As only the mixing ratio of the sum of the monoterpenes was known, an average value of the very similar NO_3 rate coefficients (IUPAC, 2019) for limonene, 3-carene and α -pinene was used for the calculation of $\sum k_i[\text{VOC}]_i$ with $k_{\text{monoterpenes}} = 9.1 \times 10^{-12} \text{ cm}^3\text{molecule}^{-1}\text{s}^{-1}$ (analogously averaged uncertainty of 47%). Figure 5 indicates very good agreement between measured and calculated NO_3 reactivity, with ~ 70% of the overall reactivity caused by isoprene, which is indicated by the purple, shaded area. Despite being present at much lower mixing ratios than isoprene, the terpenes contribute ~ 30% to the overall NO_3 reactivity, which reflects the large rate constants for reaction of NO_3 with terpenes.

The experiments described above indicate that, for a chemical system containing initially only isoprene as the reactive organic trace gas, the measured values of k^{NO_3} can be fully assigned to the isoprene present in the chamber over the course of its degradation. During the NO3ISOP campaign, not only NO_3 reactivity but also OH-reactivity (k^{OH}) was measured; the experimental technique is described briefly in the supplementary information. A detailed analysis of the OH-reactivity dataset will be subject of a further publication and in Fig. S1 we only compare values of k^{NO_3} and k^{OH} obtained directly after isoprene injections, where k^{OH} should not be significantly influenced by the reaction of OH with secondary products. As shown in Fig. S2, isoprene concentrations derived from both k^{NO_3} and k^{OH} are generally in good agreement when [isoprene] < 5 ppbv.

The oxidation of isoprene by NO_3 in air results in the formation of stable (non-radical) products as well as organic peroxy radicals (RO_2) that can also react with NO_3 . As radicals (e.g. NO_3 , RO_2 and HO_2) are not sampled by the FT-CRDS, the equivalence of k^{NO_3} and $k_5[\text{isoprene}]$ indicates that non-radical, secondary oxidation products do not contribute significantly to the NO_3 reactivity.

3.2 Steady-state and model calculations: Role of RO_2 & chamber walls

The contribution of RO_2 , HO_2 and stable products to NO_3 reactivity was examined using a box-model based on the chemical mechanistic oxidation processes of isoprene by NO_3 , OH and O_3 as incorporated in the Master Chemical Mechanism, version 3.3.1 (Saunders et al., 2003; Jenkin et al., 2015; Khan et al., 2015). A numerical simulation (Fig. 6) of the evolution of NO_3 reactivity was initialised using the experimental conditions of the first isoprene injection on 10th August (5.5 ppbv NO_2 , 60 ppbv O_3 and 2 ppbv isoprene, dry air) including chamber-specific parameters such as temperature, the NO_3 and N_2O_5 wall loss rates (quantified in detail below) and the dilution rate. In the model, NO_3 reacts both with stable products and peroxy radicals. One of several ~~The~~ major, stable oxidation products according to MCM is an organic nitrate with aldehyde functionality ($\text{O}_2\text{NOC}_4\text{H}_6\text{CHO}$, NC4CHO). As the corresponding rate coefficient for the reaction of this molecule with NO_3 is not known, MCM uses a generic rate coefficient based on the IUPAC-recommended, temperature-dependent expression for acetaldehyde + NO_3 scaled with a factor of 4.25 to take differences in molecular structure into account. The maximum, modelled mixing ratio of NC4CHO was ~ 5 ppbv in type 2 experiments which would result in a NO_3 reactivity of 0.001 s^{-1} . This value is below

the instrument's LOD and would only become observable at extremely low isoprene concentrations. As apparent in Fig. 6, the contribution of stable oxidation products (blue) to the NO₃ reactivity is insignificant compared to the primary oxidation of isoprene (red).

Since the rate coefficients for reaction of isoprene derived peroxy radicals and NO₃ are (unlike NO₃ + HO₂) poorly constrained by experimental data, the MCM uses a generic value of $2.3 \times 10^{-12} \text{ cm}^3\text{molecule}^{-1}\text{s}^{-1}$ which is based on rate coefficient for the reaction between NO₃ and C₂H₅O₂. The modelled, overall NO₃ reactivity when reactions with RO₂ and HO₂ are included (black line) is on average 22% higher than the reactivity associated only with isoprene, the major contributors to the additional NO₃ reactivity being nitrooxy isopropyl peroxy radicals (O₂NOC₅H₈O₂, NISOPOO) formed in the primary oxidation step. As neither RO₂ nor HO₂ radicals will survive the inlet tubing (and heated glass flask) between the SAPHIR chamber and the FT-CRDS instrument, our measurement of k^{NO_3} does not include their contribution. The measured values of k^{NO_3} (black datapoints) scatter around the isoprene-induced reactivity (red) which is understood to result from the minor role of stable (non-radical) oxidation products (blue) in removing NO₃ and the exclusion of peroxy radicals in the measurement.

Another method of deriving NO₃ reactivity is to calculate it from NO₃ (and/or N₂O₅) mixing ratios and production rates under the assumption of steady-state as has been carried out on several occasions for the analysis of ambient NO₃ measurements (Heintz et al., 1996; Geyer and Platt, 2002; Brown et al., 2004; Sobanski et al., 2016b). In contrast to our direct measurement of k^{NO_3} , all loss processes (including reaction of NO₃ with RO₂, HO₂ and uptake of NO₃ and N₂O₅ to surfaces) are assessed using the steady-state calculations. A comparison between k^{NO_3} and NO₃ reactivity based on a steady-state analysis should enable us to extract the contribution of peroxy radicals and wall-losses of NO₃ in the SAPHIR chamber. In steady-state, the NO₃ reactivity ($k_{\text{ss}}^{\text{NO}_3}$) is derived from the ratio between the NO₃-production rate via reaction (R2) with rate coefficient k_2 and the mixing ratios of O₃, NO₂ and NO₃ (Eq.2).

$$k_{\text{ss}}^{\text{NO}_3} = \frac{k_2[\text{O}_3][\text{NO}_2]}{[\text{NO}_3]} \quad (2)$$

Acquiring steady-state can take several hours if the NO₃ lifetime is long, temperatures are low or NO₂ mixing ratios are high (Brown et al., 2003). In the NO₃ISOP experiments, the NO₃ reactivities were generally high, and steady-state is achieved within a few minutes of isoprene being injected into the chamber. However, NO₂ re-injections in the chamber during periods of low reactivity at the end of an experiment when isoprene was already depleted can lead to a temporary breakdown of the steady-state assumption. In order to circumvent this potential source of error the non-steady-state reactivities ($k_{\text{nss}}^{\text{NO}_3}$) based on NO₃ and N₂O₅ measurements (McLaren et al., 2010) were calculated using Eq. (3).

$$k_{\text{nss}}^{\text{NO}_3} = \frac{k_2[\text{O}_3][\text{NO}_2] - \frac{d[\text{NO}_3]}{dt} - \frac{d[\text{N}_2\text{O}_5]}{dt}}{[\text{NO}_3]} \quad (3)$$

This expression is similar to Eq. (2) except for the subtraction of the derivatives $d[\text{NO}_3]/dt$ and $d[\text{N}_2\text{O}_5]/dt$ from the production term. A comparison of $k_{\text{ss}}^{\text{NO}_3}$ and $k_{\text{nss}}^{\text{NO}_3}$ is given in the SI and verifies the assumptions above: As soon as isoprene is injected into the system $k_{\text{ss}}^{\text{NO}_3}$ and $k_{\text{nss}}^{\text{NO}_3}$ are equivalent (see Fig. S3a) but $k_{\text{ss}}^{\text{NO}_3}$ shows short-term deviations at NO₂ reinjections (see Fig. S3b). As the non-steady-state reactivities are less affected by such events, the latter were used for the comparison with the

measured NO₃ reactivities. The steady-state as well as the non-steady-state calculations are only valid if equilibrium between NO₃ and N₂O₅ is established. Moreover, the N₂O₅ measurements are usually less sensitive to instrument-specific losses under dry conditions. For this reason, measured NO₃ mixing ratios were checked for consistency with the equilibrium to N₂O₅ using the equilibrium constant K_{eq} for reactions (R3)/(R4) as well as the measured N₂O₅ and NO₂ mixing ratios as denoted in Eq.

(4) for this analysis. **In case a significant deviation was observed, NO₃ mixing ratios from [NO₂], [N₂O₅] and K_{eq} were used.**

$$[\text{NO}_3]_{eq} = \frac{[\text{N}_2\text{O}_5]}{K_{eq}[\text{NO}_2]} \quad (4)$$

A time series of measured k^{NO_3} and calculated $k_{\text{nss}}^{\text{NO}_3}$ is depicted in Fig. 7a, which shows the results from experiments in the absence of aerosol only. It is evident that $k_{\text{nss}}^{\text{NO}_3}$ is much higher than k^{NO_3} . In Fig. 7b we plot k^{NO_3} versus $k_{\text{nss}}^{\text{NO}_3}$: An unweighted, orthogonal, linear fit has a slope of 0.54 ± 0.01 and indicates that the measured values of k^{NO_3} are almost a factor of two lower than $k_{\text{nss}}^{\text{NO}_3}$. Propagation of the uncertainties in k_2 (15%; IUPAC, 2019) and the NO₃, NO₂ and O₃ mixing ratios (25%, 9% and 5%, respectively) results in an overall uncertainty of 31% for $k_{\text{nss}}^{\text{NO}_3}$ which cannot account for its deviation to k^{NO_3} .

The fact that $k_{\text{nss}}^{\text{NO}_3}$ is significantly larger than k^{NO_3} indicates that NO₃ can be lost by reactions other than those with reactive, stable VOCs that can be sampled by the FT-CRDS instrument. As discussed above, RO₂ represents the most likely candidate to account for some additional loss of NO₃; the numerical simulations (MCM v3.3.1) predict an additional reactivity in the order of ~22% based on a generic value for $k_{\text{NO}_3+\text{RO}_2}$. However, in order to bring k^{NO_3} and $k_{\text{nss}}^{\text{NO}_3}$ into agreement, either the RO₂ level or the rate coefficient for reaction between NO₃ and RO₂ (especially NISOPOO) would have to be a factor of 2 larger than incorporated into the model (see below). Alternatively, losses of NO₃ (and N₂O₅) to surfaces enhance $k_{\text{nss}}^{\text{NO}_3}$ but not k^{NO_3} . As no aerosol was present in the experiments analysed above, the only surface available is provided by the chamber walls.

In order to quantify the contribution of NO₃ and N₂O₅ wall losses to $k_{\text{nss}}^{\text{NO}_3}$, we analysed the experiments from the 1st and 2nd August during isoprene-free periods, i.e. when no RO₂ radicals are present and (in the absence of photolysis and NO) uptake of NO₃ (or N₂O₅) to the chamber walls represents the only significant sink. Consequently, plotting $k_{\text{nss}}^{\text{NO}_3}$ from this period against $K_{eq}[\text{NO}_2]$ enables separation of direct NO₃ losses (R10) from indirect losses via N₂O₅ uptake (R9) and to derive first-order loss rates $k_{\text{NO}_3}^{\text{wall}}$ and $k_{\text{N}_2\text{O}_5}^{\text{wall}}$ of NO₃ and N₂O₅ according to Eq. (5). (Allan et al., 2000; Brown et al., 2009b; Crowley et al., 2010; McLaren et al., 2010).

$$k_{\text{nss}}^{\text{NO}_3} = k_{\text{wall}}^{\text{NO}_3} + k_{\text{wall}}^{\text{N}_2\text{O}_5} K_{eq}[\text{NO}_2] \quad (5)$$

The results from the isoprene-free periods of experiments on the 1st and 2nd of August are shown in Fig. 8. A linear regression of the data yields a slope $k_{\text{wall}}^{\text{N}_2\text{O}_5}$ of $(3.28 \pm 1.15) \times 10^{-4} \text{ s}^{-1}$ and an intercept $k_{\text{wall}}^{\text{NO}_3}$ of $(0.0016 \pm 0.0001) \text{ s}^{-1}$, indicating that NO₃ losses dominate and that heterogeneous removal of N₂O₅ does not contribute significantly to the overall loss rate constant of ~0.002 s⁻¹. The data reproducibility from one experiment to the next indicates that the NO₃/N₂O₅ wall loss rates are unchanged if the experimental conditions, i.e. dry air and no aerosols, are comparable. Humidification of the air on the other hand may facilitate heterogeneous reactions of NO₃ or N₂O₅ with the chamber walls and increase corresponding loss rates. This might

be an explanation for observation of a larger difference between k^{NO_3} and $k_{\text{nss}}^{\text{NO}_3}$ during an experiment under humid conditions on the 6th August (Fig. 7b, blue triangles). Lack of extensive isoprene-free periods on this day impede the extraction of wall loss rates with this approach: Even after subtraction of k^{NO_3} from $k_{\text{nss}}^{\text{NO}_3}$ equation (5) is not applicable in experiments once isoprene is present (and becomes the dominant sink of NO_3) as reactions of RO_2 indirectly co-determine the NO_2 mixing ratios. For further analysis, the wall loss rate constants of NO_3 and N_2O_5 were fixed as long as there was neither humidity nor particles in the chamber and are considered invariant with time after isoprene injections. This implicitly assumes that low volatility oxidation products that deposit on chamber walls do not enhance the reactivity of the walls to NO_3 . As these products have less double bonds than isoprene and react only very slowly with NO_3 , this assumption would appear reasonable.

We examined the effect of introducing the NO_3 and N_2O_5 wall loss rate constants calculated as described above into the chemical scheme used in the box model (Model 1, MCM v3.3.1). The results from three different model outputs for the experiment on the 2nd August are summarised in Fig. 9 which compares simulated and measured mixing ratios of NO_3 , N_2O_5 , NO_2 , O_3 and isoprene (following its addition at 11:00) as well as the measured and non-steady-state NO_3 reactivities k^{NO_3} and $k_{\text{nss}}^{\text{NO}_3}$. The omission of $\text{NO}_3/\text{N}_2\text{O}_5$ wall losses (Model 1) results in simulated NO_3 and N_2O_5 mixing ratios up to 1400 and 1600 pptv during the isoprene-free period, which exceed measurements by factors of 4-8. This is because the only loss process for these species in this phase is the dilution rate that is two orders of magnitude lower than the estimated wall loss rates. Such high amounts of $\text{NO}_3/\text{N}_2\text{O}_5$ in the ppbv range results in rapid depletion of nearly half of the total injected isoprene within the first minute which is why Model 1 cannot describe the measurements either before or after the injection. Model 2 (red lines) includes the estimated wall loss rates and reproduces the measurements more accurately: The NO_2 and O_3 mixing ratios are accurately simulated. Furthermore, NO_3 and N_2O_5 mixing ratios that are only 10 to 30% higher than those measured and therefore NO_3 reactivities lower than $k_{\text{nss}}^{\text{NO}_3}$ (orange circles) are predicted. We note that, in these isoprene-free phases, the omission of wall losses results in model predictions of NO_3 and N_2O_5 mixing ratios up to 1400 and 1600 pptv, which exceed measurements by factors of 4-8, as illustrated in (Fig. S3).

The evolution of the isoprene mixing ratio is reproduced by the model which is why k^{NO_3} , (mostly determined by $k_5[\text{isoprene}]$, (purple area)), is only slightly lower than the simulated overall reactivity by Model 2. After quantification of $\text{NO}_3/\text{N}_2\text{O}_5$ wall losses, NO_3+RO_2 reactions remain the only source of additional NO_3 reactivity to explain the difference between k^{NO_3} and $k_{\text{nss}}^{\text{NO}_3}$. As already mentioned above, the model may underestimate the effect of RO_2 induced losses of NO_3 either because the RO_2 mixing ratios are underestimated or because the rate coefficient $k_{\text{RO}_2+\text{NO}_3}$ is larger than assumed.

The result of a simulation (Model 3) with $k_{\text{RO}_2+\text{NO}_3}$ set to $4.6 \times 10^{-12} \text{ cm}^3\text{molecule}^{-1}\text{s}^{-1}$ (twice the generic value in MCM v3.3.1) is displayed as the blue lines in Fig. 9. The O_3 , NO_2 , N_2O_5 and isoprene mixing ratios are only slightly affected by this change in the reaction constant, whereas its impact on the NO_3 mixing ratios as well as on the reactivity is very significant. The higher rate coefficient for reaction of NO_3 with RO_2 would be sufficient to not only explain the observed discrepancy between the overall reactivity $k_{\text{nss}}^{\text{NO}_3}$ and k^{NO_3} within the uncertainties associated with the analysis, but also results in a better reproduction of the NO_3 measurement during the isoprene-dominated period. Optimum agreement irrespective of uncertainties

would be achieved with a value of $9.2 \times 10^{-12} \text{ cm}^3 \text{ molecule}^{-1} \text{ s}^{-1}$ for $k_{\text{RO}_2+\text{NO}_3}$ (i.e. a factor of 4 higher than in MCM) which is demonstrated in a comparable experiment under dry conditions on the 10th August (see Fig. S4 in the supplement).

There are only few experimental studies on reactions of NO_3 with RO_2 and the rate coefficient for reaction of NO_3 with isoprene-derived RO_2 has never been measured. For the reaction between NO_3 and the methyl peroxy radical (CH_3O_2) values
425 between 1.0 and $2.3 \times 10^{-12} \text{ cm}^3 \text{ molecule}^{-1} \text{ s}^{-1}$ have been reported (Crowley et al., 1990; Biggs et al., 1994; Daele et al., 1995; Helleis et al., 1996; Vaughan et al., 2006), with a preferred value of $1.2 \times 10^{-12} \text{ cm}^3 \text{ molecule}^{-1} \text{ s}^{-1}$ (Atkinson et al., 2006). Increasing the length of the C-C backbone in the peroxy radical appears to increase the rate coefficient, with values of $2.3 \times 10^{-12} \text{ cm}^3 \text{ molecule}^{-1} \text{ s}^{-1}$ preferred for reaction of NO_3 with $\text{C}_2\text{H}_5\text{O}_2$ (Atkinson et al., 2006), whereas the presence of electron-withdrawing groups attached to the peroxy-carbon atom reduces the rate coefficient (Vaughan et al., 2006). A single study of
430 the reaction between NO_3 and an acylperoxy radical indicates that the rate coefficient ($4.0 \times 10^{-12} \text{ cm}^3 \text{ molecule}^{-1} \text{ s}^{-1}$) may be larger than the MCM adopted value of $2.3 \times 10^{-12} \text{ cm}^3 \text{ molecule}^{-1} \text{ s}^{-1}$ (Canosa-Mas et al., 1996). Similarly, an indirect study (Hjorth et al., 1990) of the rate coefficient for the reaction between NO_3 and a nitro-substituted, C-6 peroxy radical, $(\text{CH}_3)_2\text{C}(\text{ONO}_2)\text{C}(\text{CH}_3)_2\text{O}_2$, reports a value of $5 \times 10^{-12} \text{ cm}^3 \text{ molecule}^{-1} \text{ s}^{-1}$ which may be appropriate for longer-chain peroxy radicals derived from biogenic trace gases. In light of the large uncertainty associated with the kinetics of $\text{RO}_2 + \text{NO}_3$ reactions,
435 a rate coefficient of $4.6 \times 10^{-12} \text{ cm}^3 \text{ molecule}^{-1} \text{ s}^{-1}$ for reaction between NISOPOO and NO_3 is certainly plausible.

We note however, that use of a faster rate coefficient for the reaction between RO_2 and NISOPOO, RO_2 isomerisation processes and differentiation between the fates of the main NISOPOO isomers as proposed by Schwantes et al. (2015) would result in lower RO_2 mixing ratios. If $k_{\text{NISOPOO}+\text{RO}_2}$ in MCM v3.3.1 is set to a value of $5 \times 10^{-12} \text{ cm}^3 \text{ molecule}^{-1} \text{ s}^{-1}$ (average over all isomers, Schwantes et al., 2015) a slightly higher value of $5.2 \times 10^{-12} \text{ cm}^3 \text{ molecule}^{-1} \text{ s}^{-1}$ for $k_{\text{RO}_2+\text{NO}_3}$ would be necessary to
440 bring modelled and measured NO_3 reactivity into agreement within associated uncertainties. Conversely, increasing RO_2 concentrations by the required factor two would necessitate a significant reduction in the model rate coefficients for $\text{RO}_2 + \text{RO}_2$ or $\text{RO}_2 + \text{HO}_2$ reactions, which contradicts experimental results (Boyd et al., 2003; Schwantes et al., 2015) and is considered unlikely.

Differences in measurement of $k_{\text{NSS}}^{\text{NO}_3}$ and modelled NO_3 reactivity could also result from incorrectly modelled product yields
445 owing to the simplified mechanism used, which does not consider in detail e.g. the formation of methyl vinyl ketone (MVK) via β -NISOPOO isomers or the reaction between NO_3 and other main products like hydroxy isopropyl nitrates (e.g. $\text{O}_2\text{NOCH}_2\text{C}(\text{CH}_3)\text{CHCH}_2\text{OH}$, ISOPCNO3) and nitrooxy isopropyl hydroperoxide ($\text{O}_2\text{NOCH}_2\text{C}(\text{CH}_3)\text{CHCH}_2\text{OOH}$, NISOPOOH). However, none of these products is expected to react sufficiently rapidly with NO_3 to make a difference: The rate coefficient for reaction of NO_3 with MVK is $< 6 \times 10^{-16} \text{ cm}^3 \text{ molecule}^{-1} \text{ s}^{-1}$ and that for 2-methyl-3-butene-2-ol (a
450 comparable molecule to ISOPCNO3) is $1.2 \times 10^{-14} \text{ cm}^3 \text{ molecule}^{-1} \text{ s}^{-1}$ at 298 K (IUPAC 2019). Even ppbv amounts of these products would not cause significant additional NO_3 reactivity.

On the other hand, the FT-CRDS will underestimate the reactivity of NO_3 if products that are formed do not make it to the inlet (i.e. trace gases with high affinity for surfaces). One potential candidate for this category is NISOPOOH, formed in the

reaction between NISOPOO and HO₂. There are no kinetic data on the reaction of NO₃ with NISOPOOH, though, given the
 455 lack of reactivity of NO₃ towards organic peroxides it is very unlikely that the rate coefficient would be larger than for NO₃ +
 O₂NOCH₂C(CH₃)=CHCHO. Analysis of one experiment (9th of August, Fig. 7b), in which HO₂ production (and thus the yield
 of NISOPOOH) was enhanced by the addition of propene and CO, shows that the difference between k^{NO_3} and $k_{nss}^{NO_3}$ on that
 day is comparable to those of the other experiments. This would also indicate that the influence of the potential non-detection
 of the hydroperoxide on the analysis should be low.

460 All in all, the results of the analysis above strongly suggest that the difference between directly measured and non-steady-state
 reactivity $k_{nss}^{NO_3}$ is caused by reactions of NO₃ with RO₂ with the results best explained when a rate coefficient of $\sim 5 \times 10^{-12}$
 cm³ molecule⁻¹ s⁻¹ is used. Quantifying the impact of peroxy radicals on the fate of NO₃ is however challenging as not only the
 rate coefficients for RO₂ + NO₃ are scarce and uncertain but also the rate constants for self-reaction of RO₂ derived from NO₃
 + isoprene have not been determined in direct kinetic measurement but via analyses of non-radical product yields.

465 4 Summary and conclusion

Direct measurements of NO₃-reactivity (k^{NO_3}) in chamber experiments exploring the NO₃ induced oxidation of isoprene
 showed excellent agreement with NO₃ loss rate constants calculated from isoprene mixing ratios, thus underlining the
 reliability of the reactivity measurements even under unfavourable conditions with as much as 25 ppbv of NO₂ in the chamber.
 The main contributor to the overall uncertainty in k^{NO_3} is the correction (via numerical simulation) for the reaction of NO₃
 470 with NO₂ and the thermal decomposition of the N₂O₅ product. The results of the NO₃ISOP campaign indicate that previously
 derived overall uncertainties (Liebmann et al., 2017) that considered an uncertainty of 10% in the rate coefficients of both
 reactions (Burkholder et al., 2015) and an 8% uncertainty for the NO₂ mixing ratios are too large.

The measured reactivity k^{NO_3} could be completely assigned to the reaction between NO₃ and isoprene, indicating that
 contributions from reactions of non-radical oxidation products are minor, which is consistent with predictions of the current
 475 version of the Master Chemical Mechanism.

Values of NO₃ reactivity as calculated from NO₃ and N₂O₅ mixing ratios and the NO₃ production term were found to be a
 factor of ~ 1.85 higher than the directly measured NO₃ reactivities k^{NO_3} . A box-model analysis indicates that the most likely
 explanation is a larger fractional loss of NO₃ via reactions with organic peroxy radicals (RO₂) formed during the oxidation of
 isoprene. A rate coefficient $k_{RO_2+NO_3} = 4.6 \times 10^{-12}$ cm³ molecule⁻¹ s⁻¹ is necessary to align model predictions (MCM v.3.3.1)
 480 and observations **within associated uncertainties**.

Acknowledgements

This work was supported by the EC Horizon 2020 project Eurochamp2020 (grant agreement no. 730997) and Labex Voltaire
 (ANR-10-LABX-100-01). This project has received funding from the European Research Council (ERC) under the European

Union's Horizon 2020 research and innovation programme (SARLEP grant agreement No. 681529). We thank Chemours for
485 provision of the FEP sample used to coat the CRD cavities and flowtube reactor.

References

- Allan, B. J., McFiggans, G., Plane, J. M. C., Coe, H., and McFadyen, G. G.: The nitrate radical in the remote marine boundary layer, *J. Geophys. Res.-Atmos.*, 105, 24191-24204, 2000.
- 490 Atkinson, R., and Arey, J.: Gas-phase tropospheric chemistry of biogenic volatile organic compounds: a review, *Atmos. Environ.*, 37, S197-S219, 2003.
- Atkinson, R., Baulch, D. L., Cox, R. A., Crowley, J. N., Hampson, R. F., Hynes, R. G., Jenkin, M. E., Rossi, M. J., and Troe, J.: Evaluated kinetic and photochemical data for atmospheric chemistry: Volume II - reactions of organic species, *Atmos. Chem. Phys.*, 3625-4055, 2006.
- 495 Biggs, P., Canosa-Mas, C. E., Fracheboud, J.-M., Shallcross, D. E., and Wayne, R. P.: Investigation into the kinetics and mechanism of the reaction of NO₃ with CH₃O₂ at 298 K and 2.5 Torr: a potential source of OH in the night-time troposphere?, *J. Chem. Soc., Faraday Trans.*, 90, 1205-1210, doi:10.1039/FT9949001205, 1994.
- 500 Bossmeyer, J., Brauers, T., Richter, C., Rohrer, F., Wegener, R., and Wahner, A.: Simulation chamber studies on the NO₃ chemistry of atmospheric aldehydes, *Geophys. Res. Lett.*, 33, 2006.
- Boyd, A. A., Flaud, P. M., Daugey, N., and Lesclaux, R.: Rate constants for RO₂ + HO₂ reactions measured under a large excess of HO₂, *J. Phys. Chem. A*, 107, 818-821, 2003.
- 505 Brown, S. S., Stark, H., and Ravishankara, A. R.: Applicability of the steady state approximation to the interpretation of atmospheric observations of NO₃ and N₂O₅, *J. Geophys. Res.-Atmos.*, 108, Art. 4539, doi:10.1029/2003JD003407, 2003.
- Brown, S. S., Dibb, J. E., Stark, H., Aldener, M., Vozella, M., Whitlow, S., Williams, E. J., Lerner, B. M., Jakoubek, R., Middlebrook, A. M., DeGouw, J. A., Warneke, C., Goldan, P. D., Kuster, W. C., Angevine, W. M., Sueper, D. T., Quinn, P. K., Bates, T. S., Meagher, J. F., Fehsenfeld, F. C., and Ravishankara, A. R.: Nighttime removal of NO_x in the summer marine boundary layer, *Geophys. Res. Lett.*, 31, Art. L07108, DOI: 07110.01029/02004GL019412, 2004.
- 510 Brown, S. S., Ryerson, T. B., Wollny, A. G., Brock, C. A., Peltier, R., Sullivan, A. P., Weber, R. J., Dube, W. P., Trainer, M., Meagher, J. F., Fehsenfeld, F. C., and Ravishankara, A. R.: Variability in nocturnal nitrogen oxide processing and its role in regional air quality, *Science*, 311, 67-70, 2006.
- 515 Brown, S. S., Degouw, J. A., Warneke, C., Ryerson, T. B., Dube, W. P., Atlas, E., Weber, R. J., Peltier, R. E., Neuman, J. A., Roberts, J. M., Swanson, A., Flocke, F., McKeen, S. A., Brioude, J., Sommariva, R., Trainer, M., Fehsenfeld, F. C., and Ravishankara, A. R.: Nocturnal isoprene oxidation over the Northeast United States in summer and its impact on reactive nitrogen partitioning and secondary organic aerosol, *Atmos. Chem. Phys.*, 9, 3027-3042, 2009a.
- 520 Brown, S. S., Dube, W. P., Fuchs, H., Ryerson, T. B., Wollny, A. G., Brock, C. A., Bahreini, R., Middlebrook, A. M., Neuman, J. A., Atlas, E., Roberts, J. M., Osthoff, H. D., Trainer, M., Fehsenfeld, F. C., and Ravishankara, A. R.: Reactive uptake coefficients for N₂O₅ determined from aircraft measurements during the Second Texas Air Quality Study: Comparison to current model parameterizations, *J. Geophys. Res.-Atmos.*, 114, art. D00F10, doi:10.1029/2008JD011679, 2009b.
- 525 Brown, S. S., and Stutz, J.: Nighttime radical observations and chemistry, *Chem. Soc. Rev.*, 41, 6405-6447, 2012.
- 530 Burkholder, J. B., Sander, S. P., Abbatt, J., Barker, J. R., Huie, R. E., Kolb, C. E., Kurylo, M. J., Orkin, V. L., Wilmouth, D. M., and Wine, P. H.: Chemical Kinetics and Photochemical Data for Use in Atmospheric Studies, Evaluation No. 18, "JPL Publication 15-10, Jet Propulsion Laboratory, Pasadena, <http://jpldataeval.jpl.nasa.gov>., 2015.
- 535 Canosa-Mas, C. E., King, M. D., Lopez, R., Percival, C. J., Wayne, R. P., Shallcross, D. E., Pyle, J. A., and Daele, V.: Is the reaction between CH₃C(O)O₂ and NO₃ important in the night-time troposphere?, *J. Chem. Soc., Faraday Trans.*, 92, 2211-2222, 1996.

- Crowley, J. N., Burrows, J. P., Moortgat, G. K., Poulet, G., and LeBras, G.: Room temperature rate coefficient for the reaction between CH_3O_2 and NO_3 , *Int. J. Chem. Kinet.*, 22, 673-681, 1990.
- 540 Crowley, J. N., Schuster, G., Pouvesle, N., Parchatka, U., Fischer, H., Bonn, B., Bingemer, H., and Lelieveld, J.: Nocturnal nitrogen oxides at a rural mountain site in south-western Germany, *Atmos. Chem. Phys.*, 10, 2795-2812, 2010.
- Crowley, J. N., Thieser, J., Tang, M. J., Schuster, G., Bozem, H., Hasaynali Beygi, Z., Fischer, H., Diesch, J.-M., Drewnick, F., Borrmann, S., Song, W., Yassaa, N., Williams, J., Pöhler, D., Platt, U., and Lelieveld, J.: Variable lifetimes and loss mechanisms for NO_3 and N_2O_5 during the DOMINO campaign: Contrast between marine, urban and continental air, *Atmos. Chem. Phys.*, 11, 10863-10870, 2011.
- 545 Curtis, A. R., and Sweetenham, W. P.: Facsimile, Atomic Energy Research Establishment, Report R-12805, 1987, 1987.
- Daele, V., Laverdet, G., Lebras, G., and Poulet, G.: Kinetics of the reactions $\text{CH}_3\text{O}+\text{NO}$, $\text{CH}_3\text{O}+\text{NO}_3$, and $\text{CH}_3\text{O}_2+\text{NO}_3$, *J. Phys. Chem.*, 99, 1470-1477, doi:10.1021/j100005a017, 1995.
- 550 Dorn, H. P., Apodaca, R. L., Ball, S. M., Brauers, T., Brown, S. S., Crowley, J. N., Dubé, W. P., Fuchs, H., Häseler, R., Heitmann, U., Jones, R. L., Kiendler-Scharr, A., Labazan, I., Langridge, J. M., Meinen, J., Mentel, T. F., Platt, U., Pöhler, D., Rohrer, F., Ruth, A. A., Schlosser, E., Schuster, G., Shillings, A. J. L., Simpson, W. R., Thieser, J., Tillmann, R., Varma, R., Venables, D. S., and Wahner, A.: Intercomparison of NO_3 radical detection instruments in the atmosphere simulation chamber SAPHIR, *Atmos. Meas. Tech.*, 6, 1111-1140, doi:10.5194/amt-6-1111-2013, 2013.
- 555 Dubé, W. P., Brown, S. S., Osthoff, H. D., Nunley, M. R., Ciciora, S. J., Paris, M. W., McLaughlin, R. J., and Ravishankara, A. R.: Aircraft instrument for simultaneous, in situ measurement of NO_3 and N_2O_5 via pulsed cavity ring-down spectroscopy, *Rev. Sci. Instrum.*, 77, doi:10.1063/1.2176058, 2006.
- 560 Edwards, P. M., Aikin, K. C., Dube, W. P., Fry, J. L., Gilman, J. B., de Gouw, J. A., Graus, M. G., Hanisco, T. F., Holloway, J., Huber, G., Kaiser, J., Keutsch, F. N., Lerner, B. M., Neuman, J. A., Parrish, D. D., Peischl, J., Pollack, I. B., Ravishankara, A. R., Roberts, J. M., Ryerson, T. B., Trainer, M., Veres, P. R., Wolfe, G. M., Warneke, C., and Brown, S. S.: Transition from high- to low- NO_x control of nighttime oxidation in the southeastern US, *Nat. Geosci.*, 10, 490-+, doi:10.1038/Ngeo2976, 2017.
- 565 Fry, J. L., Brown, S. S., Middlebrook, A. M., Edwards, P. M., Campuzano-Jost, P., Day, D. A., Jimenez, J. L., Allen, H. M., Ryerson, T. B., Pollack, I., Graus, M., Warneke, C., de Gouw, J. A., Brock, C. A., Gilman, J., Lerner, B. M., Dube, W. P., Liao, J., and Welti, A.: Secondary organic aerosol (SOA) yields from NO_3 radical + isoprene based on nighttime aircraft power plant plume transects, *Atmos. Chem. Phys.*, 18, 11663-11682, doi:10.5194/acp-18-11663-2018, 2018.
- 570 Fuchs, H., Dube, W. P., Ciciora, S. J., and Brown, S. S.: Determination of inlet transmission and conversion efficiencies for in situ measurements of the nocturnal nitrogen oxides, NO_3 , N_2O_5 and NO_2 , via pulsed cavity ring-down spectroscopy, *Anal. Chem.*, 80, 6010-6017, 2008.
- 575 Fuchs, H., Ball, S. M., Bohn, B., Brauers, T., Cohen, R. C., Dorn, H. P., Dube, W. P., Fry, J. L., Häseler, R., Heitmann, U., Jones, R. L., Kleffmann, J., Mentel, T. F., Musgen, P., Rohrer, F., Rollins, A. W., Ruth, A. A., Kiendler-Scharr, A., Schlosser, E., Shillings, A. J. L., Tillmann, R., Varma, R. M., Venables, D. S., Tapia, G. V., Wahner, A., Wegener, R., Wooldridge, P. J., and Brown, S. S.: Intercomparison of measurements of NO_2 concentrations in the atmosphere simulation chamber SAPHIR during the NO_3 -Comp campaign, *Atmos. Meas. Tech.*, 3, 21-37, 2010.
- 580 Fuchs, H., Simpson, W. R., Apodaca, R. L., Brauers, T., Cohen, R. C., Crowley, J. N., Dorn, H. P., Dubé, W. P., Fry, J. L., Häseler, R., Kajii, Y., Kiendler-Scharr, A., Labazan, I., Matsumoto, J., Mentel, T. F., Nakashima, Y., Rohrer, F., Rollins, A. W., Schuster, G., Tillmann, R., Wahner, A., Wooldridge, P. J., and Brown, S. S.: Comparison of N_2O_5 mixing ratios during NO_3 Comp 2007 in SAPHIR, *Atmos. Meas. Tech.*, 5, 2763-2777, doi:10.5194/amt-5-2763-2012, 2012.
- 585 Geyer, A., Alicke, B., Konrad, S., Schmitz, T., Stutz, J., and Platt, U.: Chemistry and oxidation capacity of the nitrate radical in the continental boundary layer near Berlin, *J. Geophys. Res.-Atmos.*, 106, 8013-8025, 2001.

- 590 Geyer, A., and Platt, U.: Temperature dependence of the NO₃ loss frequency: A new indicator for the contribution of NO₃ to the oxidation of monoterpenes and NO_x removal in the atmosphere, *J. Geophys. Res.-Atmos.*, 107, 4431, doi:10.1029/2001JD001215, doi:10.1029/2001JD001215, 2002.
- 595 Guenther, A. B., Jiang, X., Heald, C. L., Sakulyanontvittaya, T., Duhl, T., Emmons, L. K., and Wang, X.: The Model of Emissions of Gases and Aerosols from Nature version 2.1 (MEGAN2.1): an extended and updated framework for modeling biogenic emissions, *Geosci. Model. Dev.*, 5, 1471-1492, doi:10.5194/gmd-5-1471-2012, 2012.
- Heintz, F., Platt, U., Flentje, H., and Dubois, R.: Long-term observation of nitrate radicals at the tor station, Kap Arkona (Rugen), *J. Geophys. Res.-Atmos.*, 101, 22891-22910, 1996.
- 600 Helleis, F., Moortgat, G. K., and Crowley, J. N.: Kinetic investigations of the reaction of CD₃O₂ with NO and NO₃ at 298 K, *J. Phys. Chem.*, 100, 17846-17854, 1996.
- Hjorth, J., Lohse, C., Nielsen, C. J., Skov, H., and Restelli, G.: Products and Mechanisms of the Gas-Phase Reactions between NO₃ and a Series of Alkenes, *J. Phys. Chem.*, 94, 7494-7500, doi:DOI 10.1021/j100382a035, 1990.
- 605 Hohaus, T., Kuhn, U., Andres, S., Kaminski, M., Rohrer, F., Tillmann, R., Wahner, A., Wegener, R., Yu, Z., and Kiendler-Scharr, A.: A new plant chamber facility, PLUS, coupled to the atmosphere simulation chamber SAPHIR, *Atmos. Meas. Tech.*, 9, 1247-1259, doi:10.5194/amt-9-1247-2016, 2016.
- 610 Holzinger, R.: PTRwid: A new widget tool for processing PTR-TOF-MS data, *Atmos. Meas. Tech.*, 8, 3903-3922, doi:10.5194/amt-8-3903-2015, 2015.
- 615 Holzinger, R., Acton, W. J. F., Bloss, W. J., Breitenlechner, M., Crilley, L. R., Dusanter, S., Gonin, M., Gros, V., Keutsch, F. N., Kiendler-Scharr, A., Kramer, L. J., Krechmer, J. E., Languille, B., Locoge, N., Lopez-Hilfiker, F., Materic, D., Moreno, S., Nemitz, E., Quelevar, L. L. J., Esteve, R. S., Sauvage, S., Schallhart, S., Sommariva, R., Tillmann, R., Wedel, S., Worton, D. R., Xu, K. M., and Zaytsev, A.: Validity and limitations of simple reaction kinetics to calculate concentrations of organic compounds from ion counts in PTR-MS, *Atmos. Meas. Tech.*, 12, 6193-6208, doi:10.5194/amt-12-6193-2019, 2019.
- 620 IUPAC: Task Group on Atmospheric Chemical Kinetic Data Evaluation, (Ammann, M., Cox, R.A., Crowley, J.N., Herrmann, H., Jenkin, M.E., McNeill, V.F., Mellouki, A., Rossi, M. J., Troe, J. and Wallington, T. J.) <http://iupac.pole-ether.fr/index.html>, 2019.
- Jenkin, M. E., Young, J. C., and Rickard, A. R.: The MCM v3.3.1 degradation scheme for isoprene, *Atmos. Chem. Phys.*, 15, 11433-11459, doi:10.5194/acp-15-11433-2015, 2015.
- 625 Khan, M. A. H., Cooke, M. C., Utembe, S. R., Archibald, A. T., Derwent, R. G., Xiao, P., Percival, C. J., Jenkin, M. E., Morris, W. C., and Shallcross, D. E.: Global modeling of the nitrate radical (NO₃) for present and pre-industrial scenarios, *Atmos. Res.*, 164, 347-357, doi:10.1016/j.atmosres.2015.06.006, 2015.
- 630 Krechmer, J., Lopez-Hilfiker, F., Koss, A., Hutterli, M., Stoermer, C., Deming, B., Kimmel, J., Warneke, C., Holzinger, R., Jayne, J., Worsnop, D., Fuhrer, K., Gonin, M., and de Gouw, J.: Evaluation of a New Reagent-Ion Source and Focusing Ion-Molecule Reactor for Use in Proton-Transfer-Reaction Mass Spectrometry, *Anal. Chem.*, 90, 12011-12018, doi:10.1021/acs.analchem.8b02641, 2018.
- 635 Lelieveld, J., Butler, T. M., Crowley, J. N., Dillon, T. J., Fischer, H., Ganzeveld, L., Harder, H., Lawrence, M. G., Martinez, M., Taraborrelli, D., and Williams, J.: Atmospheric oxidation capacity sustained by a tropical forest, *Nature*, 452, 737-740, 2008.
- Lelieveld, J., Gromov, S., Pozzer, A., and Taraborrelli, D.: Global tropospheric hydroxyl distribution, budget and reactivity, *Atmos. Chem. Phys.*, 16, 12477-12493, 2016.
- 640 Liebmann, J. M., Schuster, G., Schuladen, J. B., Sobanski, N., Lelieveld, J., and Crowley, J. N.: Measurement of ambient NO₃ reactivity: Design, characterization and first deployment of a new instrument, *Atmos. Meas. Tech.*, 2017, 1241-1258, doi:10.5194/amt-2016-381, 2017.
- 645 Liebmann, J., Karu, E., Sobanski, N., Schuladen, J., Ehn, M., Schallhart, S., Quéléver, L., Hellen, H., Hakola, H., Hoffmann, T., Williams, J., Fischer, H., Lelieveld, J., and Crowley, J. N.: Direct measurement of NO₃ radical reactivity in a boreal forest, *Atmos. Chem. Phys.*, 2018, 3799-3815, doi:10.5194/acp-18-3799-2018, 2018a.

- Liebmann, J. M., Muller, J. B. A., Kubistin, D., Claude, A., Holla, R., Plass-Dülmer, C., Lelieveld, J., and Crowley, J. N.: Direct measurements of NO₃ reactivity in and above the boundary layer of a mountaintop site: identification of reactive trace gases and comparison with OH reactivity, *Atmos. Chem. Phys.*, 18, 12045-12059, doi:10.5194/acp-18-12045-2018, 2018b.
- 650 Martinez, M., Perner, D., Hackenthal, E. M., Kulzer, S., and Schutz, L.: NO₃ at Helgoland during the NORDEX campaign in October 1996, *J. Geophys. Res.-Atmos.*, 105, 22685-22695, 2000.
- McLaren, R., Wojtal, P., Majonis, D., McCourt, J., Halla, J. D., and Brook, J.: NO₃ radical measurements in a polluted marine environment: links to ozone formation, *Atmos. Chem. Phys.*, 10, 4187-4206, doi:10.5194/acp-10-4187-2010, 2010.
- 655 Mogensen, D., Gierens, R., Crowley, J. N., Keronen, P., Smolander, S., Sogachev, A., Nölscher, A. C., Zhou, L., Kulmala, M., Tang, M. J., Williams, J., and Boy, M.: Simulations of atmospheric OH, O₃ and NO₃ reactivities within and above the boreal forest, *Atmos. Chem. Phys.*, 15, 3909-3932, doi:10.5194/acp-15-3909-2015, 2015.
- 660 Ng, N. L., Brown, S. S., Archibald, A. T., Atlas, E., Cohen, R. C., Crowley, J. N., Day, D. A., Donahue, N. M., Fry, J. L., Fuchs, H., Griffin, R. J., Guzman, M. I., Herrmann, H., Hodzic, A., Iinuma, Y., Jimenez, J. L., Kiendler-Scharr, A., Lee, B. H., Luecken, D. J., Mao, J., McLaren, R., Mutzel, A., Osthoff, H. D., Ouyang, B., Picquet-Varrault, B., Platt, U., Pye, H. O. T., Rudich, Y., Schwantes, R. H., Shiraiwa, M., Stutz, J., Thornton, J. A., Tilgner, A., Williams, B. J., and Zaveri, R. A.: Nitrate radicals and biogenic volatile organic compounds: oxidation, mechanisms, and organic aerosol, *Atmos. Chem. Phys.*, 17, 2103-2162, doi:10.5194/acp-17-2103-2017, 2017.
- 665 Paulot, F., Henze, D. K., and Wennberg, P. O.: Impact of the isoprene photochemical cascade on tropical ozone, *Atmos. Chem. Phys.*, 12, 1307-1325, 2012.
- 670 Phillips, G. J., Thieser, J., Tang, M. J., Sobanski, N., Schuster, G., Fachinger, J., Drewnick, F., Borrmann, S., Bingemer, H., Lelieveld, J., and Crowley, J. N.: Estimating N₂O₅ uptake coefficients using ambient measurements of NO₃, N₂O₅, ClNO₂ and particle-phase nitrate, *Atmos. Chem. Phys.*, 16, 13231-13249, doi:10.5194/acp-16-13231-2016, 2016.
- Ridley, B. A., Grahek, F. E., and Walega, J. G.: A small, high-sensitivity, medium-response ozone detector suitable for measurements from light aircraft, *J. Atmos. Ocean. Tech.*, 9, 142-148, 1992.
- 675 Rohrer, F., Bohn, B., Brüning, D., Johnen, F.-J., Wahner, A., and Kleffmann, J.: Characterisation of the photolytic HONO-source in the atmosphere simulation chamber SAPHIR, *Atmos. Chem. Phys.*, 5, 2189-2201, 2005.
- 680 Rollins, A. W., Kiendler-Scharr, A., Fry, J. L., Brauers, T., Brown, S. S., Dorn, H. P., Dubé, W. P., Fuchs, H., Mensah, A., Mentel, T. F., Rohrer, F., Tillmann, R., Wegener, R., Wooldridge, P. J., and Cohen, R. C.: Isoprene oxidation by nitrate radical: alkyl nitrate and secondary organic aerosol yields, *Atmos. Chem. Phys.*, 9, 6685-6703, doi:10.5194/acp-9-6685-2009, 2009.
- Saunders, S. M., Jenkin, M. E., Derwent, R. G., and Pilling, M. J.: Protocol for the development of the Master Chemical Mechanism, MCM v3 (Part A): tropospheric degradation of non-aromatic volatile organic compounds, *Atmos. Chem. Phys.*, 3, 161-180, 2003.
- 685 Schwantes, R. H., Teng, A. P., Nguyen, T. B., Coggon, M. M., Crounse, J. D., St Clair, J. M., Zhang, X., Schilling, K. A., Seinfeld, J. H., and Wennberg, P. O.: Isoprene NO₃ Oxidation Products from the RO₂ + HO₂ Pathway, *J. Phys. Chem. A*, 119, 10158-10171, doi:10.1021/acs.jpca.5b06355, 2015.
- 690 Sharkey, T. D., and Yeh, S.: Isoprene emission from plants, *Annu. Rev. Plant. Phys.*, 52, 407-436, doi:10.1146/annurev.arplant.52.1.407, 2001.
- 695 Sobanski, N., Schuladen, J., Schuster, G., Lelieveld, J., and Crowley, J. N.: A five-channel cavity ring-down spectrometer for the detection of NO₂, NO₃, N₂O₅, total peroxy nitrates and total alkyl nitrates, *Atmos. Meas. Tech.*, 9, 5103-5118, doi:10.5194/amt-9-5103-2016, 2016a.
- Sobanski, N., Tang, M. J., Thieser, J., Schuster, G., Pöhler, D., Fischer, H., Song, W., Sauvage, C., Williams, J., Fachinger, J., Berkes, F., Hoor, P., Platt, U., Lelieveld, J., and Crowley, J. N.: Chemical and meteorological influences on the lifetime of NO₃ at a semi-rural mountain site during PARADE, *Atmos. Chem. Phys.*, 16, 4867-4883, doi:10.5194/acp-16-4867-2016, 2016b.
- 700

Thieser, J., Schuster, G., Phillips, G. J., Reiffs, A., Parchatka, U., Pöhler, D., Lelieveld, J., and Crowley, J. N.: A two-channel, thermal dissociation cavity-ringdown spectrometer for the detection of ambient NO₂, RO₂NO₂ and RONO₂, *Atmos. Meas. Tech.*, 9, 553-576, 2016.

705 van Meeningen, Y., Schurgers, G., Rinnan, R., and Holst, T.: BVOC emissions from English oak (*Quercus robur*) and European beech (*Fagus sylvatica*) along a latitudinal gradient, *Biogeosciences*, 13, 6067-6080, doi:10.5194/bg-13-6067-2016, 2016.

Vaughan, S., Canosa-Mas, C. E., Pfrang, C., Shallcross, D. E., Watson, L., and Wayne, R. P.: Kinetic studies of reactions of the nitrate radical (NO₃) with peroxy radicals (RO₂): an indirect source of OH at night?, *Phys. Chem. Chem. Phys.*, 8, 3749-3760, 2006.

710 Wagner, N. L., Dube, W. P., Washenfelder, R. A., Young, C. J., Pollack, I. B., Ryerson, T. B., and Brown, S. S.: Diode laser-based cavity ring-down instrument for NO₃, N₂O₅, NO, NO₂ and O₃ from aircraft, *Atmos. Meas. Tech.*, 4, 1227-1240, doi:10.5194/amt-4-1227-2011, 2011.

715 Warneke, C., de Gouw, J. A., Goldan, P. D., Kuster, W. C., Williams, E. J., Lerner, B. M., Jakoubek, R., Brown, S. S., Stark, H., Aldener, M., Ravishankara, A. R., Roberts, J. M., Marchewka, M., Bertman, S., Sueper, D. T., McKeen, S. A., Meagher, J. F., and Fehsenfeld, F. C.: Comparison of daytime and nighttime oxidation of biogenic and anthropogenic VOCs along the New England coast in summer during New England Air Quality Study 2002, *J. Geophys. Res.-Atmos.*, 109, 2004.

720 Wayne, R. P., Barnes, I., Biggs, P., Burrows, J. P., Canosamas, C. E., Hjorth, J., Lebras, G., Moortgat, G. K., Perner, D., Poulet, G., Restelli, G., and Sidebottom, H.: The Nitrate Radical - Physics, Chemistry, and the Atmosphere, *Atmos. Environ.*, 25, 1-203, 1991.

Wennberg, P. O., Bates, K. H., Crounse, J. D., Dodson, L. G., McVay, R. C., Mertens, L. A., Nguyen, T. B., Praske, E., Schwantes, R. H., Smarte, M. D., St Clair, J. M., Teng, A. P., Zhang, X., and Seinfeld, J. H.: Gas-Phase Reactions of Isoprene and Its Major Oxidation Products, *Chem. Rev.*, 118, 3337-3390, doi:10.1021/acs.chemrev.7b00439, 2018.

725

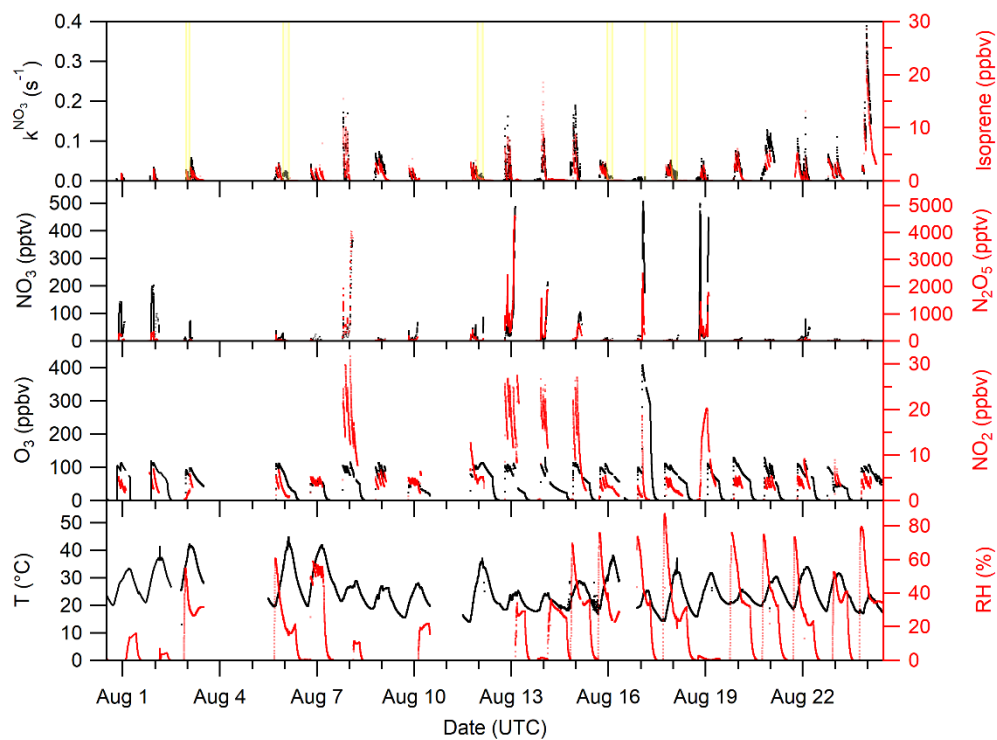
730

735

Table 1. Experimental conditions in the SAPHIR chamber during the NO3ISOP campaign.

Date	T (°C)	H ₂ O (%)	D/N	O ₃ (ppbv)	NO ₂ (ppbv)	Isoprene (ppbv)	Seed aerosol	Notes
31 July	25-35	0	N	90-120	1-5	0	--	
1 August	22-31	0	N	85-115	2-5	1.5 1.2	--	
2 August	23-38	0	N	85-120	2-5	3 2.5	--	
3 August	30-42	1.3-2.7	D->N	45-100	1-5	3 2.5	--	
6 August	20-44	1.4	N->D	40-110	1-6	3.2	--	
7 August	20-41	0.45-0.6	N	45-60	3-4.5	2.3	--	contamination
8 August	22-28	0	N	75-115	13-30	8	--	
9 August	20-27	0	N	65-115	6-2.5	3	--	CO & propene
10 August	17-28	0	N	40-65	3-5.5	2.3 1.8	--	
12 August	14-36	0	N->D	70-115	4-12	3	--	CO
13 August	28-24	0	N	75-110	12-23	8 6	--	
14 August	18-24	0	N	70-110	13-22	11 13	(NH ₄) ₂ SO ₄	Reduced fan operation
15 August	20-28	1.3-2	N	80-115	8-21	7 9	(NH ₄) ₂ SO ₄	
16 August	20-28	1.6	N->D	80-115	2-5	2.5 3	(NH ₄) ₂ SO ₄	
17 August	18-26	1.2-1.7	N->D	0-400	0-17	2.5 0	--	Isobutyl nitrate, calibration
18 August	14-31	1.3-1.4	N->D	80-110	2-5	2.5 3.5	(NH ₄) ₂ SO ₄	β-caryophyllene
19 August	16-31	0.07	N	0-110	0-20	2.3 3	(NH ₄) ₂ SO ₄	MVK, N ₂ O ₅ as NO ₂ source
20 August	20-26	1.2-19	N	85-130	3-5	4.5 6	(NH ₄) ₂ SO ₄	β-caryophyllene
21 August	20-30	1.5-1.9	N	55-130	2-5	4.5	(NH ₄) ₂ SO ₄	CO & propene
22 August	18-33	1.3-17	N	75-110	2.5-8.5	4 5	(NH ₄) ₂ SO ₄	plant emissions
23 August	18-31	1.5-2.2	N	45-100	3.5-5	3 4	(NH ₄) ₂ SO ₄	
24 August	17-23	1-1.6	N	85-110	2.3-5.5	22	NH ₄ HSO ₄	β-caryophyllene

D/N denotes if the experiment was conducted with the chamber roof opened (D: daytime) or closed (N: nighttime) and in which order a transition was done. Only maximum values of measured isoprene are listed.



745 **Figure 1: Overview of the temperature (T), relative humidity (RH), VOC-induced NO_3 reactivity (k^{NO_3}) as well as the O_3 , NO_2 , NO_3 , N_2O_5 and isoprene mixing ratios during the NO3ISOP campaign. The yellow shaded area in the upper panel represent phases of the experiment when the chamber roof was opened. The ticks mark 12:00 UTC of the corresponding day.**

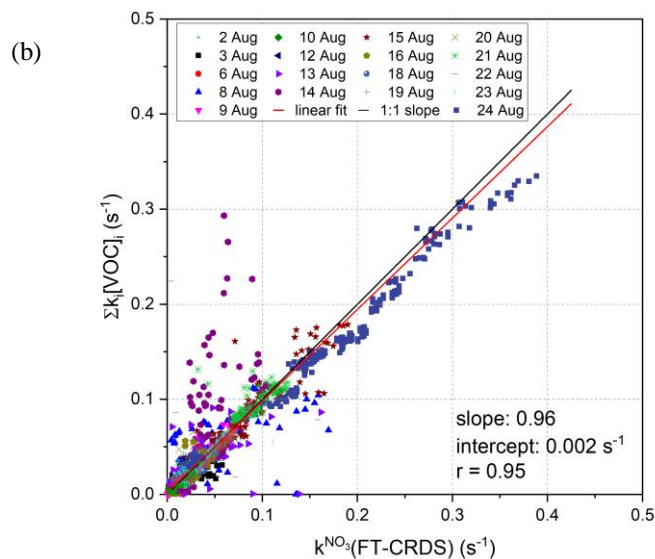
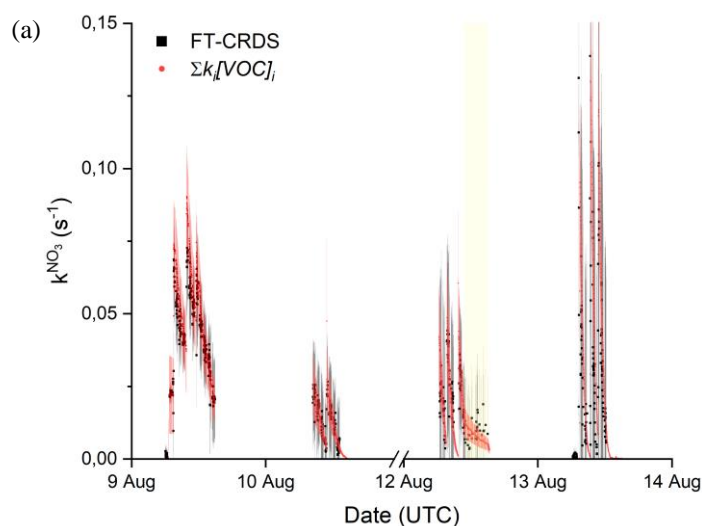


Figure 2: (a) 4-day time-series of k^{NO_3} and $\Sigma k_i[VOC]_i$. The total uncertainty in k^{NO_3} was calculated as described by Liebmann et al. (2017) and is indicated by the grey shaded area. The red shaded area shows the associated uncertainty of the calculated reactivities and are derived from error propagation using the standard deviation of the isoprene mixing ratios and an uncertainty of 41 % for the rate coefficient for reaction between NO_3 and isoprene (IUPAC, 2019). The ticks mark 00:00 UTC of the corresponding date and yellow-shaded areas represent periods in which the chamber roof was opened. (b) Correlation between $\Sigma k_i[VOC]_i$ and k^{NO_3} measurements. The red line represents a least-squares, linear fit to the entire data set, while the black line illustrates an ideal slope of 1:1.

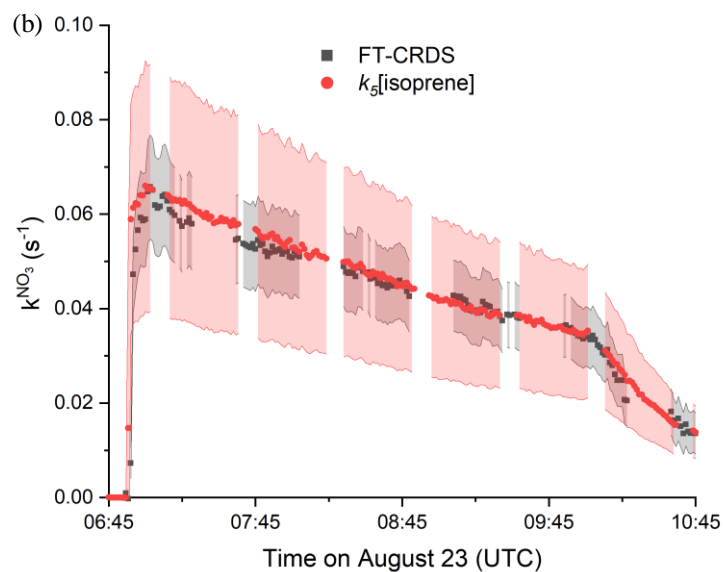
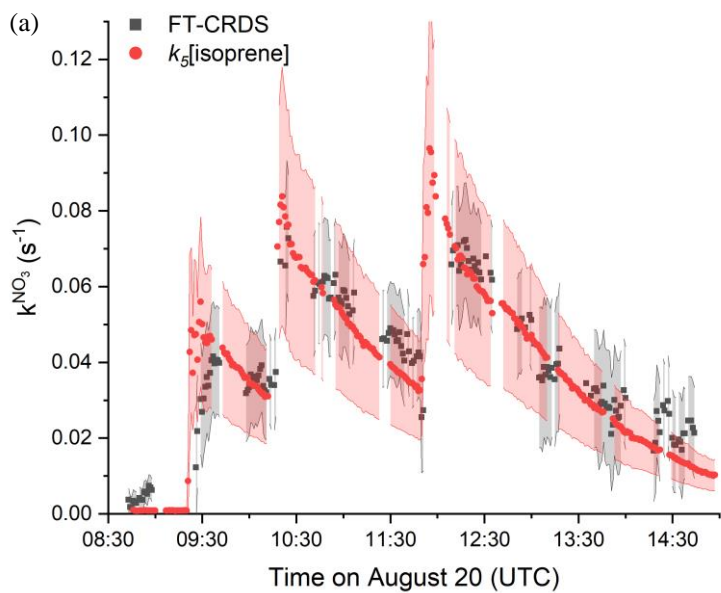
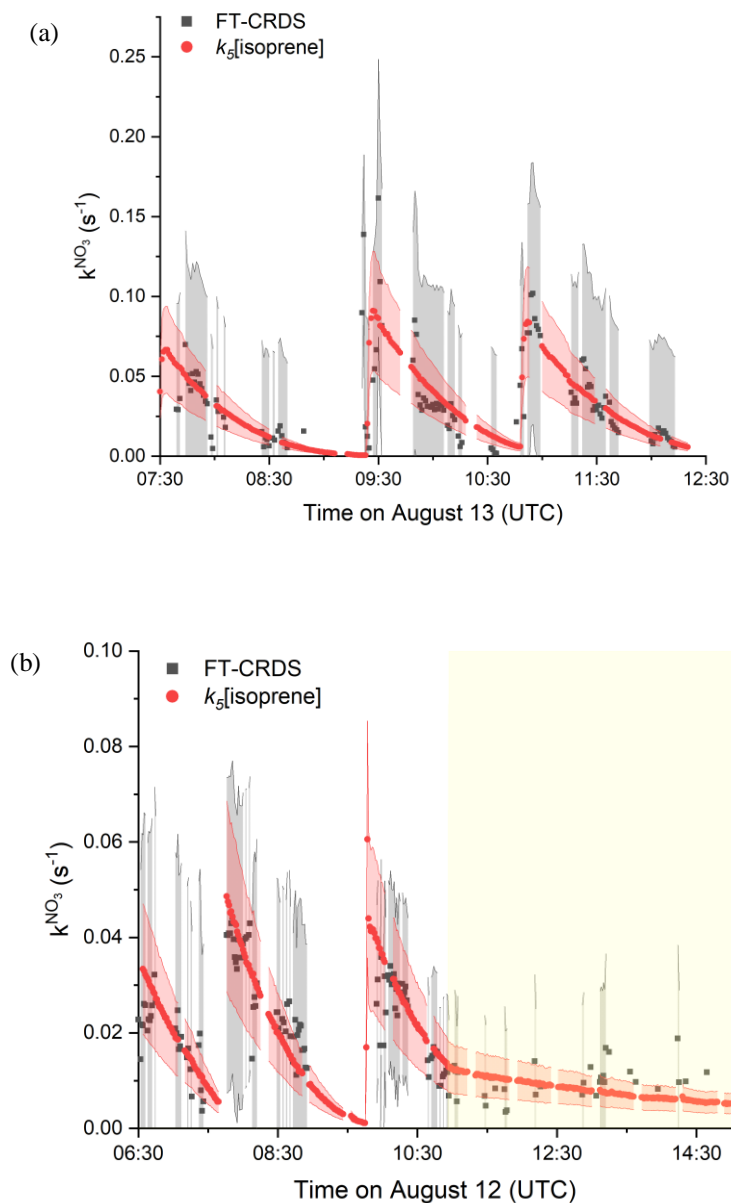


Figure 3: Measured reactivity (k^{NO_3} , black data points) and reactivity calculated from Eq. (1) (red data points) which is equivalent to $k_5[\text{isoprene}]$. The grey shaded area represents the total uncertainty in k^{NO_3} ; the red-shaded areas the total uncertainty in $k_5[\text{isoprene}]$ and were estimated as explained in Fig.2. (a) 20th August: Type 1 experiment with initial mixing ratios of $\text{NO}_2 = 4.6$ ppbv and $\text{O}_3 = 120$ ppbv. (b) 23rd August: Only O_3 (100 ppbv) and isoprene (4 ppbv) were initially present.



770 **Figure 4: Measured (black) and expected (red) NO_3 -reactivity using Eq.(1). The corresponding uncertainties were estimated as described in Fig.2 and are indicated as shaded areas. (a) Type 2 experiment from the 13th August under dry conditions with initial mixing ratios of $\text{NO}_2 = 25$ ppbv and $\text{O}_3 = 104$ ppbv. (b) Experiment from the 12th August with NO_2 mixing ratios between 7 and 12 ppbv and initial mixing ratio of $\text{O}_3 = 79$ ppbv. The yellow shaded area denotes the period with the chamber roof opened after 11:00 UTC.**

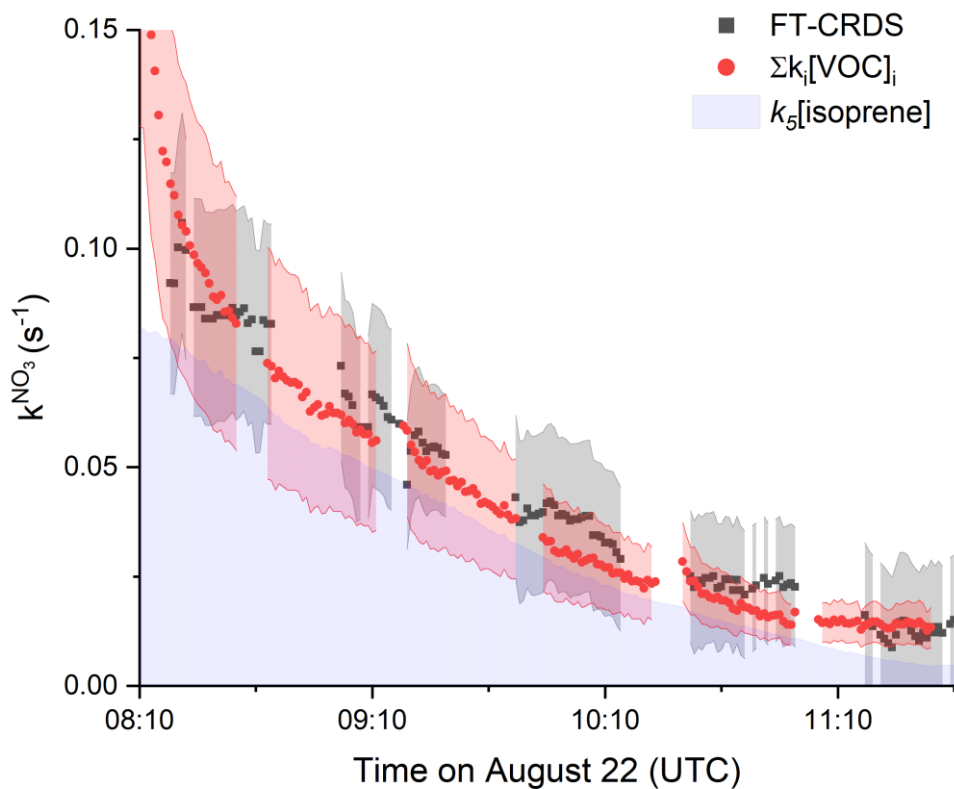


Figure 5: Results from 22nd August between 08:00 and 11:40 UTC. Comparison between k^{NO_3} (black data points, uncertainty as grey shaded area) and NO_3 reactivity calculated from $\Sigma k_i[VOC]_i$ (red data points) using the measured isoprene and Σ monoterpenes mixing ratios. The associated uncertainty (red area) was derived by error propagation considering the standard deviations of the VOC mixing ratios as well as the uncertainties of the rate coefficients (41% for k_5 and 47% for $k_{monoterpenes}$). The uncertainty of k^{NO_3} was estimated as explained in Fig.2. The contribution of isoprene to the observed reactivity is indicated by the area in purple.

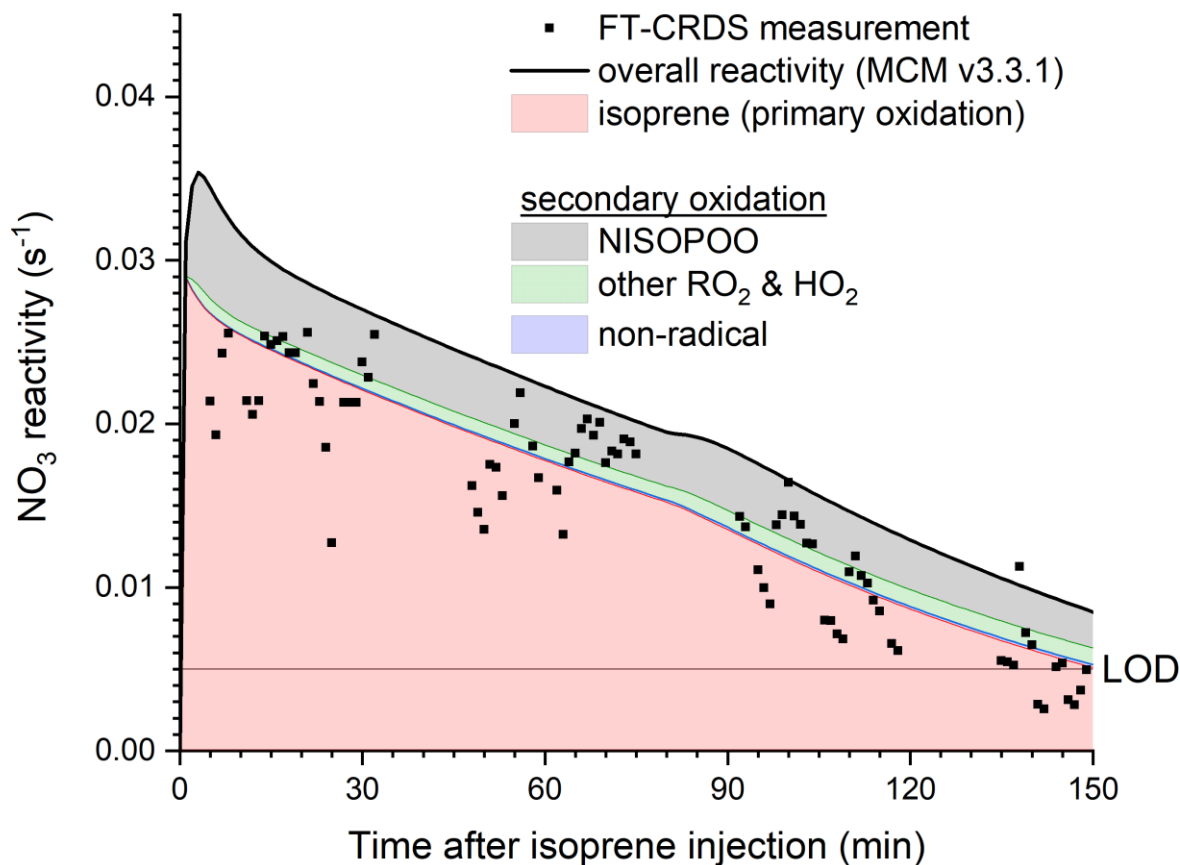


Figure 6: Experimental results for k^{NO_3} and numerical simulation (MCM v3.3.1) of the NO_3 reactivity following the first isoprene injection of the experiment on the 10th August. The simulation was run with 1 min resolution, initial conditions were 60 ppbv of O_3 , 5.5 ppbv of NO_2 and 2 ppbv of isoprene and used actual chamber temperatures, which increased from 293 to 301 K during the course of the experiment. Wall losses of NO_3 and N_2O_5 were parameterised as described in the text. Individual contributions to the NO_3 reactivity of isoprene, peroxy radicals and secondary oxidation products are highlighted.

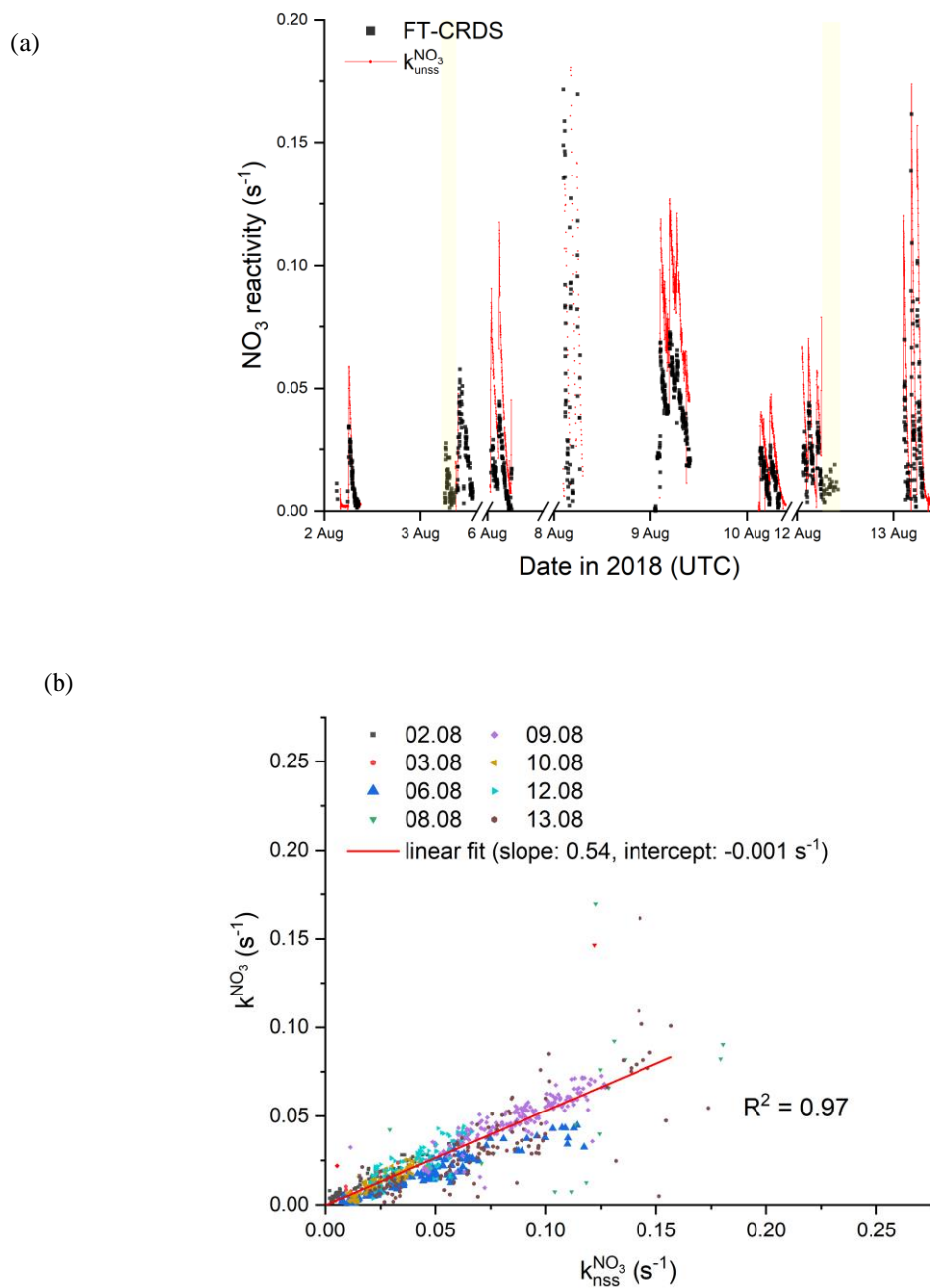
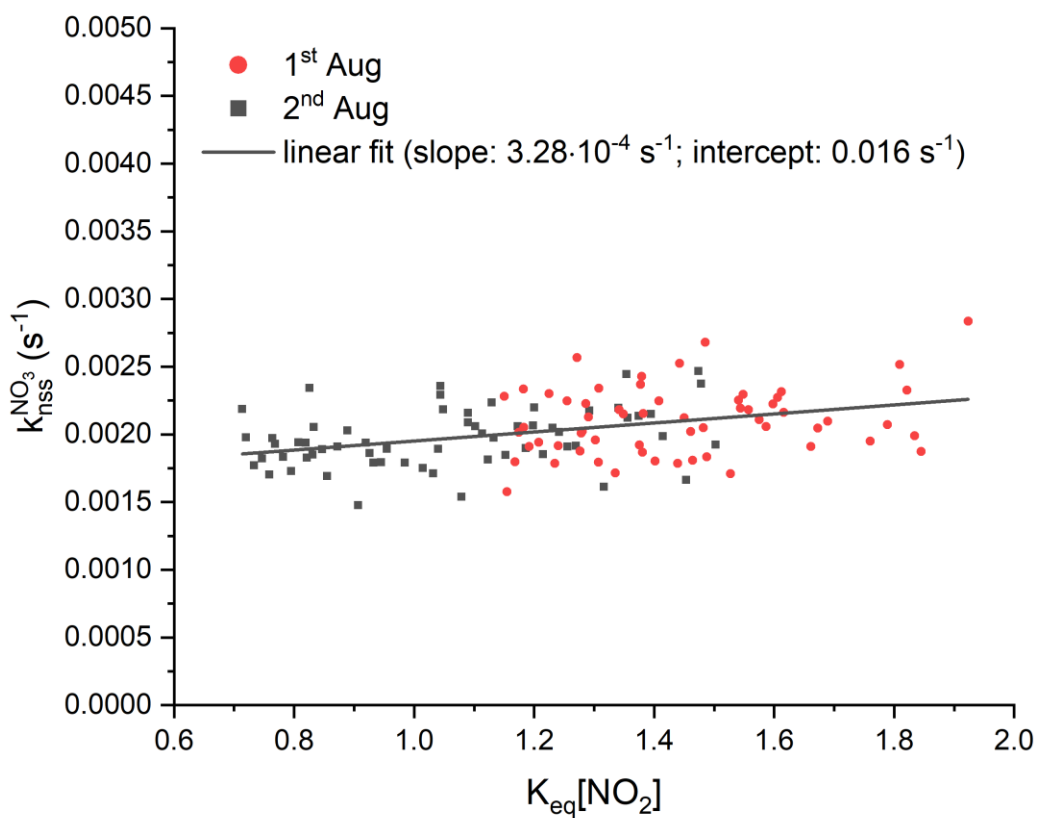


Figure 7: (a) Overview of measured (black) and calculated NO₃-reactivity with Eq. 3 (red). The ticks mark 00:00 UTC of the corresponding day. The yellow-coloured areas denote periods with an opened chamber roof. For the sake of clarity, the uncertainties are not included. (b) Correlation plot between k^{NO_3} and $k_{\text{hss}}^{\text{NO}_3}$. The red line represents an unweighted, orthogonal linear regression ($R^2 = 0.97$) of the complete dataset.



805 **Figure 8:** Analysis of the contribution of wall losses of NO_3 and N_2O_5 to NO_3 reactivity $k_{\text{nss}}^{\text{NO}_3}$ using experimental data during isoprene-free periods on the 1st (red) and 2nd (black) August. Least-squares, linear fit of the data is shown with a black line and yielded to an intercept $k_{\text{wall}}^{\text{NO}_3}$ of 0.016 s^{-1} as well as to a slope $k_{\text{wall}}^{\text{N}_2\text{O}_5}$ of $3.28 \times 10^{-4} \text{ s}^{-1}$. For sake of better clarity, error bars are not included.

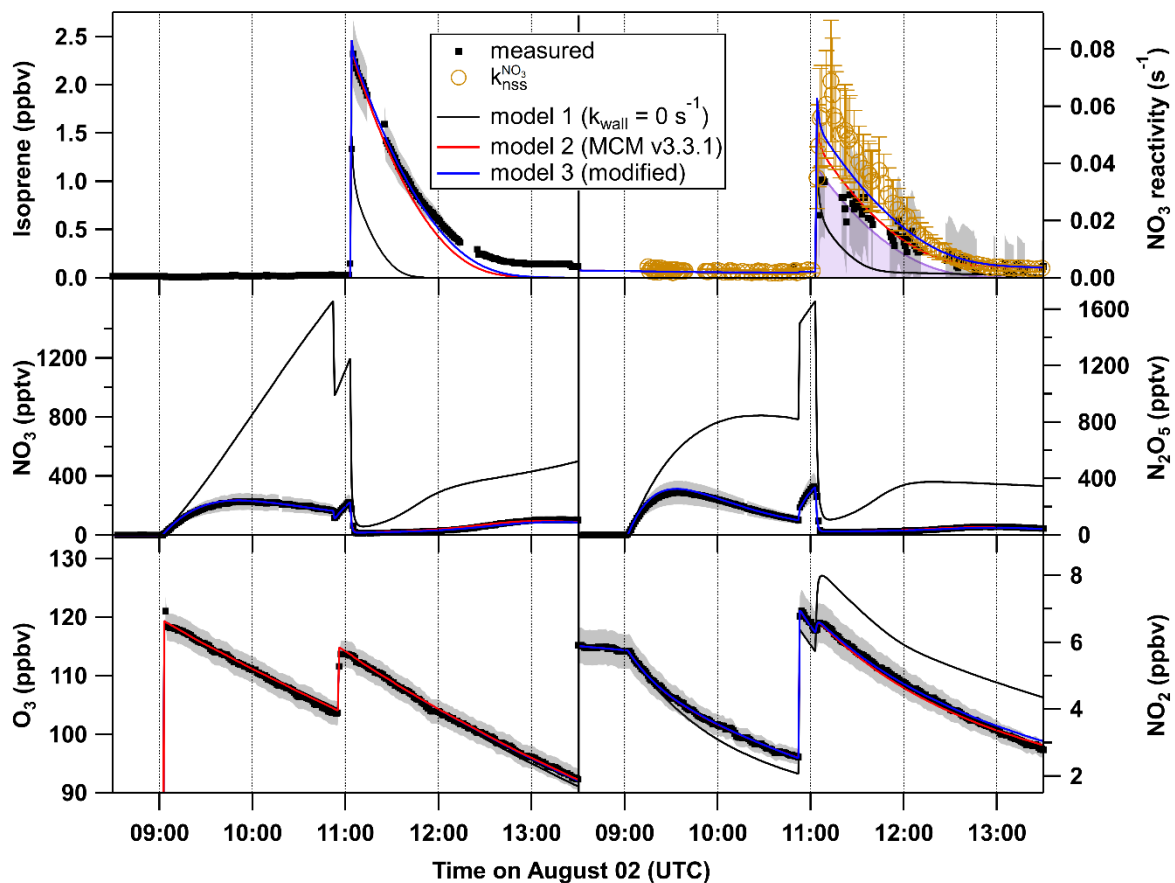


Figure 9: O₃, NO₂, NO₃, N₂O₅ and isoprene mixing ratios and NO₃ reactivity on 2nd August (black). The grey shaded area symbolizes the overall uncertainty associated with each measurement. Orange circles denote the reactivity obtained using Eq.(3). The results of the numerical simulation using MCM v3.3.1 with NO₃ and N₂O₅ wall loss rates set to 0 s⁻¹ (model 1) are shown by black lines. The model output with introduction of NO₃ and N₂O₅ wall loss rates of 0.016 s⁻¹ and 3.3 × 10⁻⁴ s⁻¹ respectively for each of the reactants is shown by a red line (model 2), whereas the blue line (model 3) shows the result of model 2 with the rate coefficient for reaction between NO₃ and RO₂ set to 4.6 × 10⁻¹² cm³molecule⁻¹s⁻¹, which is twice the value estimated by the MCM.

Evolution of NO₃ reactivity during the oxidation of isoprene

Patrick Dewald¹, Jonathan M. Liebmann¹, Nils Friedrich¹, Justin Shenolikar¹, Jan Schuladen¹, Franz Rohrer², David Reimer², Ralf Tillmann², Anna Novelli², Changmin Cho², Kangming Xu³, Rupert Holzinger³, François Bernard^{4,a}, Li Zhou⁴, Wahid Mellouki⁴, Steven S. Brown^{5,6}, Hendrik Fuchs², Jos Lelieveld¹ and John N. Crowley¹

¹Atmospheric Chemistry Department, Max Planck Institut für Chemie, 55128 Mainz, Germany

²Institute of Energy and Climate Research, IEK-8: Troposphere, Forschungszentrum Jülich GmbH, 52428 Jülich, Germany

³Institute for Marine and Atmospheric Research, IMAU, Utrecht University, Utrecht, Netherlands

⁴Institut de Combustion, Aérothermique, Réactivité et Environnement (ICARE), CNRS (UPR 3021) /OSUC, 1C Avenue de la

10 Recherche Scientifique, 45071 Orléans Cedex 2, France

⁵NOAA Chemical Sciences Laboratory, 325 Broadway, Boulder, CO 80305, USA

⁶Department of Chemistry, University of Colorado, Boulder, CO 80209, USA

^anow at: Laboratoire de Physique et Chimie de l'Environnement et de l'Espace (LPC2E), Centre National de la Recherche Scientifique (CNRS), Université d'Orléans, Observatoire des Sciences de l'Univers en région Centre - Val de Loire (OSUC),

15 Orléans, France

Correspondence to: John N. Crowley (john.crowley@mpic.de)

Supplementary Information

20

25

30

Table S1: Reactions, rate coefficients and definitions in the model used for analysis. The isoprene oxidation scheme until the 3rd / 4th generation from the Master Chemical Mechanism (MCM) version 3.3.1 is used (Jenkin et al., 2015). Any change from MCMv3.3.1 is annotated.

Reaction	Reaction constant	Annotations
NOx chemistry		
$\text{N}_2\text{O}_5 \rightarrow \text{NO}_3 + \text{NO}_2$	$((1.3\text{e-}3*(\text{T}/300)^{-3.5}*\exp(-11000/\text{T}))*\text{M}*(9.7\text{e}14*(\text{T}/300)^{0.1}*\exp(-11080/\text{T}))/((1.3\text{e-}3*(\text{T}/300)^{-3.5}*\exp(-11000/\text{T}))*\text{M}+(9.7\text{e}14*(\text{T}/300)^{0.1}*\exp(-11080/\text{T}))*10@(\log10(0.35)/(1+(\log10((1.3\text{e-}3*(\text{T}/300)^{-3.5}*\exp(-11000/\text{T}))*\text{M}/(9.7\text{e}14*(\text{T}/300)^{0.1}*\exp(-11080/\text{T}))))/(0.75-1.27*\log10(0.35)))@2))$	
$\text{NO}_2 + \text{NO}_3 \rightarrow \text{N}_2\text{O}_5$	$((3.6\text{e-}30*(\text{T}/300)^{-4.1})*\text{M}*(1.9\text{e-}12*(\text{T}/300)^{0.2}))/((3.6\text{e-}30*(\text{T}/300)^{-4.1})*\text{M}+(1.9\text{e-}12*(\text{T}/300)^{0.2}))*10@(\log10(0.35)/(1+(\log10((3.6\text{e-}30*(\text{T}/300)^{-4.1})*\text{M}/(1.9\text{e-}12*(\text{T}/300)^{0.2}))/((0.75-1.27*\log10(0.35)))@2))$	
$\text{NO} + \text{O}_3 \rightarrow \text{NO}_2 + \text{O}_2$	$1.8\text{E-}11*\exp(110/\text{T})$	
$\text{NO}_2 + \text{O}_3 \rightarrow \text{NO}_3 + \text{O}_2$	$1.4\text{E-}13 * \exp (-2470/\text{T})$	
$\text{NO} + \text{O}_3 \rightarrow \text{NO}_2 + \text{O}_2$	$2.07\text{E-}12 * \exp (-1400/\text{T})$	
$\text{NO}_3 + \text{CO} \rightarrow$	$4\text{E-}19$	Hjorth et al., 1986
$\text{OH} + \text{NO}_2 \rightarrow \text{HNO}_3$	$((3.2\text{e-}30*(\text{T}/300)^{-4.5})*\text{M}*(3.0\text{e-}11))/((3.2\text{e-}30*(\text{T}/300)^{-4.5})*\text{M}+(3.0\text{e-}11))*10@(\log10(0.41)/(1+(\log10((3.2\text{e-}30*(\text{T}/300)^{-4.5})*\text{M}/(3.0\text{e-}11))/((0.75-1.27*\log10(0.41)))@2))$	
$\text{OH} + \text{NO}_3 \rightarrow \text{HO}_2 + \text{NO}_2$	$2\text{E-}11$	
$\text{HO}_2 + \text{NO}_3 \rightarrow \text{OH} + \text{NO}_2$	$4\text{E-}12$	
$\text{OH} + \text{NO} \rightarrow \text{HONO}$	$((7.4\text{e-}31*(\text{T}/300)^{-2.4})*\text{M}*(3.3\text{e-}11*(\text{T}/300)^{-0.3}))/((7.4\text{e-}31*(\text{T}/300)^{-2.4})*\text{M}+(3.3\text{e-}11*(\text{T}/300)^{-0.3}))*10@(\log10(0.81)/(1+(\log10((7.4\text{e-}31*(\text{T}/300)^{-2.4})*\text{M}/(3.3\text{e-}11*(\text{T}/300)^{-0.3}))/((0.75-1.27*\log10(0.81)))@2))$	
$\text{HO}_2 + \text{NO} \rightarrow \text{OH} + \text{NO}_2$	$3.45\text{E-}12*\exp(270/\text{T})$	
$\text{HO}_2 + \text{NO}_2 \rightarrow \text{HO}_2\text{NO}_2$	$((1.4\text{e-}31*(\text{T}/300)^{-3.1})*\text{M}*(4.0\text{e-}12))/((1.4\text{e-}31*(\text{T}/300)^{-3.1})*\text{M}+(4.0\text{e-}12))*10@(\log10(0.4)/(1+(\log10((1.4\text{e-}31*(\text{T}/300)^{-3.1})*\text{M}/(4.0\text{e-}12))/((0.75-1.27*\log10(0.4)))@2))$	
$\text{HO}_2\text{NO}_2 + \text{OH} \rightarrow \text{NO}_2$	$3.2\text{e-}13*\text{EXP}(690/\text{T})$	
$\text{HO}_2\text{NO}_2 \rightarrow \text{HO}_2 + \text{NO}_2$	$((4.1\text{e-}5*\exp(-10650/\text{T}))*\text{M}*(6.0\text{e}15*\exp(-11170/\text{T}))/((4.1\text{e-}5*\exp(-10650/\text{T}))*\text{M}+(6.0\text{e}15*\exp(-11170/\text{T}))*10@(\log10(0.4)/(1+(\log10((4.1\text{e-}5*\exp(-10650/\text{T}))*\text{M}/(6.0\text{e}15*\exp(-11170/\text{T}))/((0.75-1.27*\log10(0.4)))@2))$	

OH + HONO → NO ₂	2.5e-12*EXP(260/T)	
OH + HNO ₃ → NO ₃	2.40E-14*EXP(460/T) + ((6.50E-34*EXP(1335/T)*M)/ (1+(6.50E-34*EXP(1335/T)*M/2.70E-17*EXP(2199/T))))	
HOx chemistry		
OH + O ₃ → HO ₂	1.70E-12*EXP(-940/T)	
HO ₂ + O ₃ → OH	2.03E-16*(T/300)@4.57*EXP(693/T)	
OH + HO ₂ →	4.8E-11*EXP(250/T)	
HO ₂ + HO ₂ → H ₂ O ₂	2.20E-13*(1+(1.40E-21*EXP(2200/T)*H ₂ O))*EXP(600/T)	
OH + H ₂ O ₂ → HO ₂	2.9E-12*exp(-160/T)	
OH + CO → HO ₂	1.44E-13*(1+(M/4.2E19))	
Primary oxidation of isoprene		
NO ₃ + C ₅ H ₈ → NISOP ₂	2.95E-12 * exp (-450/T)	IUPAC, 2019
O ₃ + C ₅ H ₈ → CH ₂ O ₂ + MACR	0.3 * 1.03E-14 * exp (-1995/T)	
O ₃ + C ₅ H ₈ → CH ₂ O ₂ + MVK	0.2 * 1.03E-14 * exp (-1995/T)	
O ₃ + C ₅ H ₈ → HCHO + MACROOA	0.3 * 1.03E-14 * exp (-1995/T)	
O ₃ + C ₅ H ₈ → HCHO + MVKOOA	0.2 * 1.03E-14 * exp (-1995/T)	
OH + C ₅ H ₈ → CISOPA	0.288*2.7E-11 * exp (390/T)	
OH + C ₅ H ₈ → CISOPC	0.238*2.7E-11 * exp (390/T)	
OH + C ₅ H ₈ → ISOP34O ₂	0.022*2.7E-11 * exp (390/T)	
OH + C ₅ H ₈ → ME3BU3ECHO + HO ₂	0.02*2.7E-11 * exp (390/T)	
OH + C ₅ H ₈ → PE4E2CO + HO ₂	0.042*2.7E-11 * exp (390/T)	
OH + C ₅ H ₈ → TISOPA	0.288*2.7E-11 * exp (390/T)	
OH + C ₅ H ₈ → TISOPC	0.102*2.7E-11 * exp (390/T)	
Secondary oxidation (1st generation)		
NISOP ₂ + HO ₂ → NISOP ₂ OOH	0.706*2.91E-13 * EXP(1300/T)	
NISOP ₂ + NO ₃ → NISOP ₂ + NO ₂	2.3E-12	
NISOP ₂ + RO ₂ → ISOPCNO ₃	0.2*1.3E-12	
NISOP ₂ + RO ₂ → NC4CHO	0.2*1.3E-12	
NISOP ₂ + RO ₂ → NISOP ₂	0.6*1.3E-12	
CH ₂ O ₂ → CH ₂ O	0.22*1E6	
CH ₂ O ₂ → CO	0.51*1E6	
CH ₂ O ₂ → HO ₂ + CO + OH	0.27*1E6	
MACR + NO ₃ → MACO ₃ + HNO ₃	3.4E-15	

MACR + O3 → HCHO + MGLYOOb	0.12*1.4E-15*EXP(-2100/T)	
MACR + O3 → MGLYOX + CH2OOG	0.88*1.4E-15*EXP(-2100/T)	
MACR + OH → MACO3	0.45*8.0E-12*EXP(380/T)	
MACR + OH → MACRO2	0.47*8.0E-12*EXP(380/T)	
MACR + OH → MACROHO2	0.08*8.0E-12*EXP(380/T)	
MVK + O3 → MGLOOA + HCHO	0.5*8.5E-16*EXP(-1520/T)	
MVK + O3 → MGLYOX + CH2OOb	0.5*8.5E-16*EXP(-1520/T)	
MVK + OH → HVMKAO2	0.3*2.6E-12*EXP(610/T)	
MVK + OH → HVMKBO2	0.7*2.6E-12*EXP(610/T)	
HCHO + NO3 → HNO3 + CO + HO2	5.5E-16	
HCHO + OH → HO2 + CO	5.4E-12 * exp (135/T)	
MACROOA → C3H6	0.255*1E6	
MACROOA → CH3CO3 + HCHO + HO2	0.255*1E6	
MACROOA → MACROO	0.22*1E6	
MACROOA → OH + CO +CH3CO3 + HCHO	0.27*1E6	
MVKOOA → C3H6	0.255*1E6	
MVKOOA → CH3O2 + HCHO + CO + HO2	0.255*1E6	
MVKOOA → MVKOO	0.22*1E6	
MVKOOA → OH + MVKO2	0.27*1E6	
CISOPA + O2 → CISOPAO2	3.5E-12	
CISOPA + O2 → ISOPBO2	3E-12	
CISOPC + O2 → CISOPCO2	2E-12	
CISOPC + O2 → ISOPDO2	3.5E-12	
ISOP34O2 + HO2 → ISOP34OOH	2.91E-13 * EXP(1300/T)	
ISOP34O2 + NO3 → ISOP34O + NO2	2.3E-12	
ISOP34O2 + RO2 → HC4CHO	0.1*2.65E-12	
ISOP34O2 + RO2 → ISOP34O	0.8*2.65E-12	
ISOP34O2 + RO2 → ISOPDOH	0.1*2.65E-12	
ME3BU3ECHO + NO3 → NC526O2	3.3E-13	

ME3BU3ECHO + O3 → CH2OOC + CO2C3CHO	0.33*1.6E-17	
ME3BU3ECHO + O3 → HCHO + CO2C3OOB	0.67*1.6E-17	
ME3BU3ECHO + OH → C530O2	0.712*7.3E-11	
ME3BU3ECHO + OH → ME3BU3ECO3	0.288*7.3E-11	
PE4E2CO + NO3 → NC51O2	1.2E-14	
PE4E2CO + O3 → CH2OOB + CO2C3CHO	0.43*1E-17	
PE4E2CO + O3 → HCHO + CO2C3OOA	0.57*1E-17	
PE4E2CO + OH → C51O2	2.71E-11	
TISOPA + O2 → ISOPAO2	2.5E-12*exp(-480/T)	
TISOPA + O2 → ISOPBO2	3E-12	
TISOPC + O2 → ISOPCO2	2.5E-12*exp(-480/T)	
TISOPC + O2 → ISOPDO2	3.5E-12	
Secondary oxidation (2nd generation)		
NISOPOOH + OH → NC4CHO + OH	1.03E-10	
NISOPO + O2 → NC4CHO + HO2	2.50E-14*EXP(-300/T)	
ISOPCNO3 + OH → INCO2	1.12E-10	
NC4CHO + NO3 → NC4CO3 + HNO3	4.25*1.4E-12*EXP(-1860/T)	
NC4CHO + OH → C510O2	0.52*4.16E-11	
NC4CHO + OH → NC4CO3	0.48*4.16E-11	
NC4CHO + O3 → NOA + GLYOOC	0.5*2.4E-17	
NC4CHO + O3 → GLYOX + NOA00A	0.5*2.4E-17	
CH2OO + CO → HCHO	1.2E-15	
CH2OO + NO2 → HCHO + NO3	1E-15	
MACO3 + NO3 → CH3C2H2O2 + NO2	1.74 * 2.3E-12	
MACO3 + HO2 → CH3C2H2O2	0.44 * 5.2E-13*EXP(980/T)	
MACO3 + HO2 →	0.66 5.2E-13*EXP(980/T)	
MACO3 + RO2 → CH3C2H2O2	0.7*1E-11	
MACO3 + RO2 →	0.3*1E-11	

MGLYOOB → MGLYOO	0.18*1E6	
MGLYOOB → OH + CO + CH3CO3	0.82*1E6	
MGLYOX + NO3 → CH3CO3 + CO + HNO3	2.4*1.4E-12*EXP(-1860/T)	
MGLYOX + OH → CH3CO3 + CO	1.9E-12*exp(575/T)	
CH2OOG → CH2OO	0.37*1E6	
CH2OOG → CO	0.47*1E6	
CH2OOG → HO2 + CO + OH	0.16*1E6	
MACRO2 + HO2 → MACROOH	0.625*2.91E-13 * EXP(1300/T)	
MACRO2 + NO3 → MACRO + NO2	2.3E-12	
MACRO2 + RO2 → ACETOL	9.2E-14	
MACROHO2 + HO2 → (MACROHOOH)	0.625*2.91E-13 * EXP(1300/T)	
MACROHO2 + NO3 → MACROHO + NO2	2.3E-12	
MACROHO2 + RO2 → (div)	1.4E-12	
MGLOOA → CH3CHO	0.2*1E6	
MGLOOA → OH + CO + CH3CO3	0.36*1E6	
MGLOOA → CH3CO3 + HCHO + HO2	0.2*1E6	
MGLOOA → MGLOO	0.24*1E6	
CH2OOB → CH2OO	0.24*1E6	
CH2OOB → CO	0.4*1E6	
CH2OOB → HO2 + CO + OH	0.36*1E6	
HMVKA02 + HO2 → (HMTKAOOH)	0.625*2.91E-13 * EXP(1300/T)	
HMVKA02 + NO3 → NO2 + HMTKAO	2.3E-12	
HMVKA02 + RO2 → (div)	2E-12	
HMTKBO2 + HO2 → (HMTKBOOH)	0.625*2.91E-13 * EXP(1300/T)	
HMTKBO2 + NO3 → NO2 + HMTKBO	2.3E-12	
HMTKBO2 + RO2 → (div)	8.8E-13	
C3H6 + O3 → CH2OOB + CH3CHO	0.5*5.5E-15*EXP(-1880/T)	

C3H6 + O3 → CH3CHOOA + HCHO	0.5*5.5E-15*EXP(-1880/T)	
C3H6 + NO3 → PRONO3AO2	0.35*4.6E-13*EXP(-1155/T)	
C3H6 + NO3 → PRONO3BO2	0.65*4.6E-13*EXP(-1155/T)	
C3H6 + OH → HYPROPO2	0.87* ((8e-27*(T/300)@-3.5)*M*(3.0e-11*(T/300)@-1))/ ((8e-27*(T/300)@-3.5)*M+(3.0e-11*(T/300)@-1))* 10@(log10(0.5)/(1+(log10((8e-27*(T/300)@-3.5)*M/ (3.0e-11*(T/300)@-1)))/(0.75-1.27*log10(0.5))))@2))	
C3H6 + OH → IPROPOLO2	0.13* ((8e-27*(T/300)@-3.5)*M*(3.0e-11*(T/300)@-1))/ ((8e-27*(T/300)@-3.5)*M+(3.0e-11*(T/300)@-1))* 10@(log10(0.5)/(1+(log10((8e-27*(T/300)@-3.5)*M/ (3.0e-11*(T/300)@-1)))/(0.75-1.27*log10(0.5))))@2))	
CH3CO3 + HO2 → CH3CO2H + O3	5.2E-13*EXP(980/T)	
CH3CO3 + NO3 → NO2 + CH3O2	4E-12	
CH3CO3 + RO2 → CH3CO2H	0.3*1E-11	
CH3CO3 + RO2 → CH3O2	0.7*1E-11	
MACROO + CO → MACR	1.2e-15	
MACROO + NO2 → MACR + NO3	1E-15	
CH3O2 + HO2 →	3.8E-13*EXP(780/T)*(1-1/(1+498*EXP(-1160/T)))	
CH3O2 + HO2 → HCHO	3.8E-13*EXP(780/T)*(1/(1+498*EXP(-1160/T)))	
CH3O2 + NO3 → CH3O + NO2	1.2E-12	
CH3O2 + RO2 → CH3OH	0.5* 2*1.03E-13*EXP(365/T)*0.5*(1-7.18*EXP(-885/T))	
CH3O2 + RO2 → HCHO	0.5* 2*1.03E-13*EXP(365/T)*0.5*(1-7.18*EXP(-885/T))	
MVKOO + CO → MVK	1.2E-15	
MVKOO + NO2 → MVK + NO3	1E-15	
MVKO2 + HO2 → (MVKOOH)	0.625*2.91E-13 * EXP(1300/T)	
MVKO2 + NO3 → NO2	2.3E-12	
MVKO2 + RO2 → (div)	2E-12	
CISOPAO2 + HO2 → ISOPAOOH	0.706*2.91E-13 * EXP(1300/T)	
CISOPAO2 + NO3 → CISOPAO + NO2	2.3E-12	
CISOPAO2 → C536O2	0.5*2.20E10*EXP(-8174/T)*EXP(1.00E8/T@3)	
CISOPAO2 → C5HPALD1 + HO2	0.5*2.20E10*EXP(-8174/T)*EXP(1.00E8/T@3)	
CISOPAO2 → CISOPA	5.22E15*EXP(-9838/T)	
CISOPAO2 + RO2 → CISOPAO	0.8*2.4E-12	

CISOPAO2 + RO2 → HC4ACHO	0.1*2.4E-12	
CISOPAO2 + RO2 → ISOPAOH	0.1*2.4E-12	
ISOPBO2 + HO2 → ISOPBOOH	0.706*2.91E-13 * EXP(1300/T)	
ISOPBO2 + NO3 → ISOPBO + NO2	2.3E-12	
ISOPBO2 + RO2 → ISOPBO	0.8*8E-13	
ISOPBO2 + RO2 → ISOPBOH	0.2*8E-13	
CISOPCO2 + HO2 → ISOPCOOH	0.706*2.91E-13 * EXP(1300/T)	
CISOPCO2 + NO3 → CISOPCO + NO2	2.3E-12	
CISOPCO2 → C537O2	0.5*2.20E10*EXP(-8174/T)*EXP(1.00E8/T@3)	
CISOPCO2 → C5HPALD2 + HO2	0.5*2.20E10*EXP(-8174/T)*EXP(1.00E8/T@3)	
CISOPCO2 → CISOPC	3.06E15*EXP(-10254/T)	
CISOPCO2 + RO2 → CISOPCO	0.8*2E-12	
CISOPCO2 + RO2 → HC4CCHO	0.2*2E-12	
CISOPCO2 + RO2 → ISOPAOH	0.2*2E-12	
ISOPDO2 + HO2 → ISOPDOOH	0.706*2.91E-13 * EXP(1300/T)	
ISOPDO2 + NO3 → ISOPDO + NO2	2.3E-12	
ISOPDO2 + RO2 → ISOPDO	0.8*2.9E-12	
ISOPDO2 + RO2 → HCOC5	0.1*2.9E-12	
ISOPDO2 + RO2 → ISOPDOH	0.1*2.9E-12	
ISOP34OOH + OH → HC4CHO + OH	9.73E-11	
ISOP34O → MACR + HCHO + HO2	1E6	
HC4CHO + OH → C58O2	0.829*1.04E-10	
HC4CHO + OH → HC4CO3	0.171*1.04E-10	
ISOPDOH + OH → HCOC5 + HO2	7.38E-11	
NC526O2 + NO3 → NO2 +	2.3E-12	
NC526O2 + RO2 →	9.20E-14	
CH2OOC → CH2OO	0.18*1E6	
CH2OOC → HO2 + CO + OH	0.82*1E6	
CO2C3CHO + NO3 → HNO3 + CO2C3CO3	4* 1.4E-12*EXP(-1860/T)	

CO ₂ C ₃ CHO + OH → CO ₂ C ₃ CO ₃	7.15E-11	
CO ₂ C ₃ O ₂ B → C ₄ CO ₂ O ₂ + OH	0.82*1E6	
CO ₂ C ₃ O ₂ B → CO ₂ C ₃ O ₂	0.18*1E6	
C ₅ 30O ₂ + HO ₂ →	0.706*2.91E-13 * EXP(1300/T)	
C ₅ 30O ₂ + NO ₃ → NO ₂ +	2.3E-12	
C ₅ 30O ₂ + RO ₂ →	9.2E-14	
ME ₃ BU ₃ ECO ₃ + HO ₂ → C ₄ 5O ₂ + OH + NO ₂	0.44*1.4E-12*EXP(-1860/T)	
ME ₃ BU ₃ ECO ₃ + HO ₂ →	0.56*2.91E-13 * EXP(1300/T)	
ME ₃ BU ₃ ECO + NO ₃ → C ₄ 5O ₂ + NO ₂	1.6*2.3E-12	
ME ₃ BU ₃ ECO ₃ + RO ₂ → C ₄ 5O ₂	1E-11	
NC ₅ 10O ₂ + HO ₂ →	0.625*2.91E-13 * EXP(1300/T)	
NC ₅ 10O ₂ + NO ₃ → NO ₂ +	2.3E-12	
NC ₅ 10O ₂ + RO ₂ →	8.8E-12	
CO ₂ C ₃ O ₂ A → C ₄ CO ₂ O ₂ + OH	0.36*1E6	
CO ₂ C ₃ O ₂ A → CH ₂ COCH ₂ O ₂ + HO ₂	0.2*1E6	
CO ₂ C ₃ O ₂ A → CH ₂ COCH ₃	0.2*1E6	
CO ₂ C ₃ O ₂ A → CO ₂ C ₃ O ₂	0.24*1E6	
C ₅ 1O ₂ + HO ₂ →	0.706*2.91E-13 * EXP(1300/T)	
C ₅ 1O ₂ + NO ₃ → NO ₂ +	2.3E-12	
ISOPAO ₂ + HO ₂ → ISOPAOOH	0.706*2.91E-13 * EXP(1300/T)	
ISOPAO ₂ + NO ₃ → NO ₂ + ISOPAO	2.3E-12	
ISOPAO ₂ + RO ₂ → HC ₄ ACHO	0.1*2.4E-12	
ISOPAO ₂ + RO ₂ → ISOPAO	0.8*2.4E-12	
ISOPAO ₂ + RO ₂ → ISOPAOH	0.1*2.4E-12	
ISOPCO ₂ + HO ₂ → ISOPCOOH	0.706*2.91E-13 * EXP(1300/T)	
ISOPCO ₂ + NO ₃ → NO ₂ + ISOPCO	2.3E-12	
ISOPCO ₂ + RO ₂ → HC ₄ CCHO	0.1*2E-12	
ISOPCO ₂ + RO ₂ → ISOPAOH	0.1*2E-12	
ISOPCO ₂ + RO ₂ → ISOPCO	0.8*2E12	
Secondary oxidation (3rd + generation)		
INCO ₂ + HO ₂ →	0.706*2.91E-13 * EXP(1300/T)	
INCO ₂ + NO ₃ → NO ₂ +	2.3E-12	
INCO ₂ + RO ₂ →	2.9E-12	

NC4CO3 + HO2 → NOA + CO+ HO2 + OH	0.44*5.2E-13*EXP(980/T)	
NC4CO3 + HO2 →	0.66*5.2E-13*EXP(980/T)	
NC4CO3 + NO3 → NOA + CO + HO2 + NO2	1.74*2.3E-12	
NC4CO3 + RO2 →	0.3*1E-11	
NC4CO3 + RO2 → NOA + HO2 + CO	0.7*1E-11	
NOA + OH → MGLYOX + NO2	1.3E-13	
C510O2 + HO2 →	0.706*2.91E-13 * EXP(1300/T)	
C510O2 + NO3 → NO2	2.3E-12	
C510O2 + RO2 →	9.2E-14	
GLYOOC → GLYOO	0.11*1E6	
GLYOOC → OH + HO2 + CO + CO	0.89*1E6	
GLYOO + NO2 → GLYOX + NO3	1E-15	
NOA00A → NOA0O	0.11*1E6	
NOA00A → OH + NO2 + MGLYOX	0.89*1E6	
NOA0O + NO2 → NOA + NO3	1E-15	
CH3C2H2O2 → CH3CO3 + HCHO	0.35*1E6	
CH3C2H2O2 → HCHO + CH3O2 + CO	0.65*1E6	
MGLYOO + NO2 → MGLYOX + NO3	1E-15	
MACROOH + OH → ACETOL + CO + OH	3.77E-11	
MACRO → ACETOL + CO+ HO2	1E6	
MACROHO → MGLYOX + HCHO + HO2	1E6	
MGLOO + NO2 → MGLYOX + NO3	1E-15	
HMVKA0 → MGLYOX + HCHO + HO2	1E6	
HMVKBO → CH3CO3 + HOCH2CHO	1E6	
CH3CHOOA → CH3CHOO	0.24*1E6	

CH ₃ CHOOA → CH ₃ O ₂ + CO + OH	0.36*1E6	
CH ₃ CHOOA → CH ₃ O ₂ + HO ₂	0.2*1E6	
CH ₃ CHOOA →	0.2*1E6	
CH ₃ CHOO + CO → CH ₃ CHO	1.2E-15	
CH ₃ CHOO + NO ₂ → CH ₃ CHO + NO ₃	1E-15	
PRONO ₃ AO ₂ + HO ₂ →	0.520*2.91E-13 * EXP(1300/T)	
PRONO ₃ AO ₂ + NO ₃ → NO ₂ +	2.3E-12	
PRONO ₃ AO ₂ + RO ₂ →	0.2*6E-13	
PRONO ₃ BO ₂ + HO ₂ →	0.520*2.91E-13 * EXP(1300/T)	
PRONO ₃ BO ₂ + NO ₃ → NO ₂ +	2.3E-12	
PRONO ₃ BO ₂ + RO ₂ →	0.2*4E-14	
HYPROPO ₂ + HO ₂ →	0.520*2.91E-13 * EXP(1300/T)	
HYPROPO ₂ + NO ₃ → NO ₂ +	2.3E-12	
HYPROPO ₂ + RO ₂ →	8.8E-13	
IPOPOLO ₂ + HO ₂ →	0.520*2.91E-13 * EXP(1300/T)	
IPOPOLO ₂ + NO ₃ → NO ₂ +	2.3E-12	
IPOPOLO ₂ + RO ₂ →	2E-12	
MVKOOH + OH → VGLYOX	2.55E-11	
MVKOOH + OH → MVKO ₂	1.90E-12*EXP(190/T)	
VGLYOX + NO ₃ →	2.0*1.4E-12*EXP(-1860/T)	
CH ₃ CO ₂ H + OH → CH ₃ O ₂	8E-13	
ISOPAOOH + OH → HC ₄ ACHO	0.05*1.54E-10	
ISOPAOOH + OH → IEPOXA + OH	0.93*1.54E-10	
ISOPAOOH + OH → ISOPAO ₂	0.02*1.54E-10	
HC ₄ ACHO + NO ₃ → HC ₄ ACO ₃ + HNO ₃	4.25*1.4E-12*EXP(-1860/T)	
HC ₄ ACHO + O ₃ → ACETOL + GLYOX	0.5*2.4E-17	
HC ₄ ACHO + O ₃ → CO +	0.5*2.4E-17	
HC ₄ ACHO + OH → C ₅ HO ₂	0.52*4.52E-11	
HC ₄ ACHO + OH → HC ₄ ACO ₃	0.49*4.52E-11	
C ₅ HO ₂ + HO ₂ →	0.706*2.91E-13 * EXP(1300/T)	
C ₅ HO ₂ + NO ₃ → NO ₂ +	2.3E-12	
C ₅ HO ₂ + RO ₂ →	9.2E-14	
HC ₄ ACO ₃ + HO ₂ →	5.2E-13*EXP(980/T)	
HC ₄ ACO ₃ + NO ₃ → NO ₂ +	1.74*2.3E-12	
HC ₄ ACO ₃ + RO ₂ →	1E-11	

HC4ACO3 → HO2 +	2.20E10*EXP(-8174/T)*EXP(1.00E8/T@3)	
CISOPAO → C526O2	0.19*1E6	
CISOPAO → HC4CCHO + HO2	0.63*1E6	
CISOPAO → HO2 + M3F	0.18*1E6	
C526O2 + HO2 →	0.706*2.91E-13 * EXP(1300/T)	
C526O2 + NO3 → NO2 +	2.3E-12	
C526O2 + RO2 →	9.20E-14	
C526O2 → CO + OH	3.00E7*EXP(-5300/T)	
M3F + NO3 → NO2 +	1.9E-11	
M3F + O3 →	2E-17	
M3F + OH → HO2 +	9E-11	
C536O2 + HO2 →	0.706*2.91E-13 * EXP(1300/T)	
C536O2 + NO3 → NO2 +	2.3E-12	
C536O2 + RO2 →	9.20E-14	
C536O2 → CO + OH	3.00E7*EXP(-5300/T)	
C5HPALD1 + NO3 → OH + HNO3 +	4.25*1.4E-12*EXP(-1860/T)	
C5HPALD1 + O3 → MGLYOOA	0.73*2.4E-17	
C5HPALD1 + O3 → MGLYOX	0.27*2.4E-17	
MGLYOOA → MGLYOO	0.11*1E6	
MGLYOOA → CH3CO3 + OH +CO	0.89*1E6	
C5HPALD1 + OH → OH +	5.2E-11	
ISOPAOH + OH → HC4ACHO+ HO2	0.5*9.3E-11	
ISOPAOH + OH → HC4CCHO + HO2	0.5*9.3E-11	
HC4CCHO + NO3 → HC4CCO3 + HNO3	4.25*1.4E-12*EXP(-1860/T)	
HC4CCHO + O3 →	2.4E-17	
HC4CCHO + OH → C57O2	0.52*4.52E-11	
HC4CCHO + OH → HC4CCO3	0.48*4.52E-11	
HC4CCO3 + HO2 →	5.2E-13*EXP(980/T)	
HC4CCO3 + NO3 → NO2 +	1.74*2.3E-12	
HC4CCO3 + RO2 →	1E-11	
C57O2 + HO2 →	0.706*2.91E-13 * EXP(1300/T)	
C57O2 + NO3 → NO2 +	2.3E-12	
C57O2 + RO2 →	9.20E-14	
ISOPBOOH + OH → IEPOXB + OH	0.92*5E-11	

ISOPBOOH + OH → ISOPBO2	0.08*5E-11	
IEPOXB + OH → IEB1O2	0.5*9.05E-12	
IEPOXB + OH → IEB2O2	0.5*9.05E-12	
IEB1O2 + HO2 →	0.706*2.91E-13 * EXP(1300/T)	
IEB1O2 + NO3 → NO2 +	2.3E-12	
IEB1O2 + RO2 →	9.20E-14	
IEB1O2 + HO2 →	0.706*2.91E-13 * EXP(1300/T)	
IEB1O2 + NO3 → NO2 +	2.3E-12	
IEB1O2 + RO2 →	8.8E-13	
ISOPBO → MVK + HCHO + HO2	1E6	
ISOPBOH + OH → ISOPBO	3.85E-11	
ISOPCOOH + OH → HC4CCHO + OH	0.05*1.54E-10	
ISOPCOOH + OH → IEPOXC + OH	0.93*1.54E-10	
ISOPCOOH + OH → ISOPCO2	0.02*1.54E-10	
IEPOXC + OH → IEC1O2	0.719*1.5E-11	
IEPOXC + OH →	0.281*1.5E-11	
IEC1O2 + HO2 →	0.706*2.91E-13 * EXP(1300/T)	
IEC1O2 + NO3 → NO2 +	2.3E-12	
IEC1O2 + RO2 →	9.2E-14	
CISOPCO → C527O2	0.3*1E6	
CISOPCO → HC4ACHO	0.52*1E6	
CISOPCO → HO2 + M3F	0.18*1E6	
C527O2 + HO2 →	0.706*2.91E-13 * EXP(1300/T)	
C527O2 + NO3 → NO2 +	2.3E-12	
C527O2 + RO2 →	8.8E-13	
C527O2 → CO + OH	3.00E7*EXP(-5300/T)	
C537O2 + HO2 →	0.706*2.91E-13 * EXP(1300/T)	
C537O2 + NO3 → NO2 +	2.3E-12	
C537O2 + RO2 →	9.2E-14	
C537O2 → CO + OH	3.00E7*EXP(-5300/T)	
C5HPALD2 + NO3 → OH + HNO3 +	4.25*1.4E-12*EXP(-1860/T)	
C5HPALD2 + O3 → MGLYOOC	0.73*2.4E-17	
C5HPALD2 + O3 → MGLYOX	0.27*2.4E-17	
C5HPALD2 + OH → OH	5.2E-11	
ISOPAOH + OH → HC4ACHO + HO2	0.5*9.3E-11	

ISOPAOH + OH → HC4CCHO + HO2	0.5*9.3E-11	
ISOPDOOH + OH → HCOC5 + OH	0.22*1.15E-10	
ISOPDOOH + OH → IEPOXB + OH	0.75*1.15E-10	
ISOPDOOH + ISOPDO2	0.03*1.15E-10	
OH + HCOC5 → C59O2	3.81E-11	
C59O2 + HO2 →	0.706*2.91E-13 * EXP(1300/T)	
C59O2 + NO3 → NO2 +	2.3E-12	
C59O2 + RO2 →	9.2E-14	
ISOPDO → MACR + HCHO + HO2	1E6	
ISOPDOH + OH → HCOC5	7.38E-11	
HC4CO3 + HO2 →	0.56*2.91E-13 * EXP(1300/T)	
HC4CO3 + HO2 → MACR + HO2 + OH	0.44*2.91E-13 * EXP(1300/T)	
HC4CO3 + NO3 → MACR + HO2 + NO2	1.5*2.3E-12	
HC4CO3 → MACR + HO2	1E-11	
CO2C3CO3 + HO2 → CH3COCH2O2	0.44*2.91E-13 * EXP(1300/T)	
CO2C3CO3 + HO2 →	0.56*2.91E-13 * EXP(1300/T)	
CO2C3CO3 + NO3 → CH3COCH2O2 + NO2	1.74*2.3E-12	
CO2C3CO3 → CH3COCH2O2	1E-11	
CH3COCH2O2 + HO2 → OH +	0.15*1.36E-13*EXP(1250/T)	
CH3COCH2O2 + HO2 →	0.85*1.36E-13*EXP(1250/T)	
CH3COCH2O2 + NO3 → NO2 +	2.3E-12	
CH3COCH2O2 + RO2 → ACETOL	0.2* 2*(3.5E-13*8E-12)@0.5	
CH3COCH2O2 + RO2 →	0.6* 2*(3.5E-13*8E-12)@0.5	
CH3COCH2O2 + RO2 → MGLYOX	0.2* 2*(3.5E-13*8E-12)@0.5	
CO2C3OO + CO →	1.2E-15	
CO2C3OO + NO2 → NO3 +	1E-15	
C4CO2O2 + HO2 →	0.625*2.91E-13 * EXP(1300/T)	
C4CO2O2 + NO3 → NO2 +	2.3E-12	
C4CO2O2 + RO2 →	8.8E-12	
C45O2 + HO2 →	0.625*2.91E-13 * EXP(1300/T)	
C45O2 + NO3 → NO2 +	2.3E-12	

C45O2 + RO2 →	1.3E-12	
ISOPAO → C524O2	0.25*1E6	
ISOPAO → HC4CHO + HO2	0.75*1E6	
C524O2 + HO2 →	0.706*2.91E-13 * EXP(1300/T)	
C5242 + NO3 → NO2 +	2.3E-12	
C5242 + RO2 →	2.9E-12	
ISOPCOOH + OH → HC4CCHO + OH	0.05*1.54E-10	
ISOPCOOH + OH → IEPOXC + OH	0.93*1.54E-10	
ISOPCOOH + ISOPCO2	0.02*1.54E-10	
ISOPCO → HC4ACHO + HO2	0.75*1E6	
ISOPCO → HC4CCHO + HO2	0.25*1E6	
β-caryophyllene		Jenkin et al., 2012
BCARY + NO3 → NBCO2	1.9E-11	
NBCO2 + NO3 →	2.3E-12	
BCARY + O3 → BCAA00	0.435*1.2E-14	
BCARY + O3 → BCBOO	0.435*1.2E-14	
BCARY + O3 →	0.13*1.2E-14	
BCAA00 → BCSOZ	8E1	
BCBOO → BCSOZ	1.2E2	
SAPHIR chamber		
Y + OH → HO2	1.44E-13*(1+(M/4.2E19))	OH background reactivity; behaving like CO (Fuchs et al., 2013)
Z + wall →	3.86E-6	Wall loss for O ₃ , H ₂ O ₂ , HO ₂ , HONO and HNO ₃ (Richter, 2007)
NO3 + wall →	1.6E-3	Wall loss NO ₃
N2O5 + wall →	3.3E-4	Wall loss N ₂ O ₅
Definitions		
RO2	NISOP02 + ISOP34O2 + CH3C2H2O2 + MACO3 + MACRO2 + MACROHO2 + CH3CO3 + HMVKA02 + HMVKBO2 + CH3O2 + MVKO2 + CISOPAO2 + ISOPBO2 + CISOPCO2 + ISOPDO2 + NC526O2 + C530O2 + M3BU3ECO3 + C45O2 + NC51O2 + C51O2 + ISOPAO2 + ISOPCO2 + INCO2 + NC4CO3 + C510O2 + PRONO3AO2 + PRONO3BO2 + HYPROPO2 + IPROPOLO2 + C536O2 + C537O2 + INAO2 + C58O2 + HC4CO3 + CO2C3CO3 + CH3COCH2O2 + C4CO2O2 + C527O2 + C526O2 + HC4ACO3 HC4CCO3 + C57O2 + C59O2 + C524O2	organic peroxides
kNO3_all	C5H8*2.95E-12*exp(450/T) + BCARY*1.9E-11 + C3H6*4.6E-13*exp(-1155/T) + (2.3E-12*(NISOP02 + ISOPAO2 +	overall NO ₃ reactivity

	<p>ISOPBO2 + ISOPCO2 + ISOPDO2 + CH3C2H2O2 + MACO3 + MACRO2 + MACROHO2 + HMKAO2 + HMKBO2 + MVKO2 + INCO2 + CISOPAO + CISOPAO2 + (NC4CO3*1.74) + C510O2 + NBCO2 + PRONO3AO2 + PRONO3BO2 + HYPROPO2 + IPROPOLO2 + INAO2 + C524O2 + (HC4ACO3*1.74) + (1.6*HC4CO3) + C58O2 + INB1O2 + (HC4CCO3*2.74) + INDO2 + C57O2 + C59O2 + C51O2 + IEB1O2 + IEB2O2 + IEC1O2 + ISOP34O2 + CISOPCO2 + NC526O2 + C527O2 + C526O2 + C536O2 + C537O2 + C530O2 + C45O2 + 1.6*M3BU3ECO3 + INB2O2 + NC51O2 + 1.74*CO2C3CO3 + CH3COCH2O2 + C4CO2O2)) + (4E-12*CH3CO3) + (1.2E-12*CH3O2) + (HO2*4E-12) + (5.5E-16*HCHO) + (4E-19*CO) + 1.4E-12*EXP(-1860/T)*(NC4CHO*4.25 + HC4ACHO*4.25 + HC4CCHO*4.25 + 2.4*MGLYOX + 4*CO2C3CHO + 4.25*C5HPALD1 + 4.25*C5HPALD2 +2*VGLYOX) + 3.3E-13*ME3BU3ECHO + (M3F*1.9E-11) + (1.2E-14*PE4E2CO)</p>	
kNO3_stable	<p>C5H8*2.95E-12*exp(450/T) + BCARY*1.9E-11 + C3H6*4.6E-13*exp(-1155/T) + (5.5E-16*HCHO) + (4E-19*CO) + 1.4E-12*EXP(-1860/T)*(NC4CHO*4.25 + HC4ACHO*4.25 + HC4CCHO*4.25 + 2.4*MGLYOX + 4*CO2C3CHO + 4.25*C5HPALD1 + 4.25*C5HPALD2 +2*VGLYOX) + 3.3E-13*ME3BU3ECHO + (M3F*1.9E-11) + (1.2E-14*PE4E2CO)</p>	NO ₃ reactivity measurable by FT-CRDS
M	<p>P*(3.24E16)*(298/T)</p>	Total molecular concentration using measured pressure P in Torr and temperature T in K

40

45

Exemplary comparison of isoprene measurements

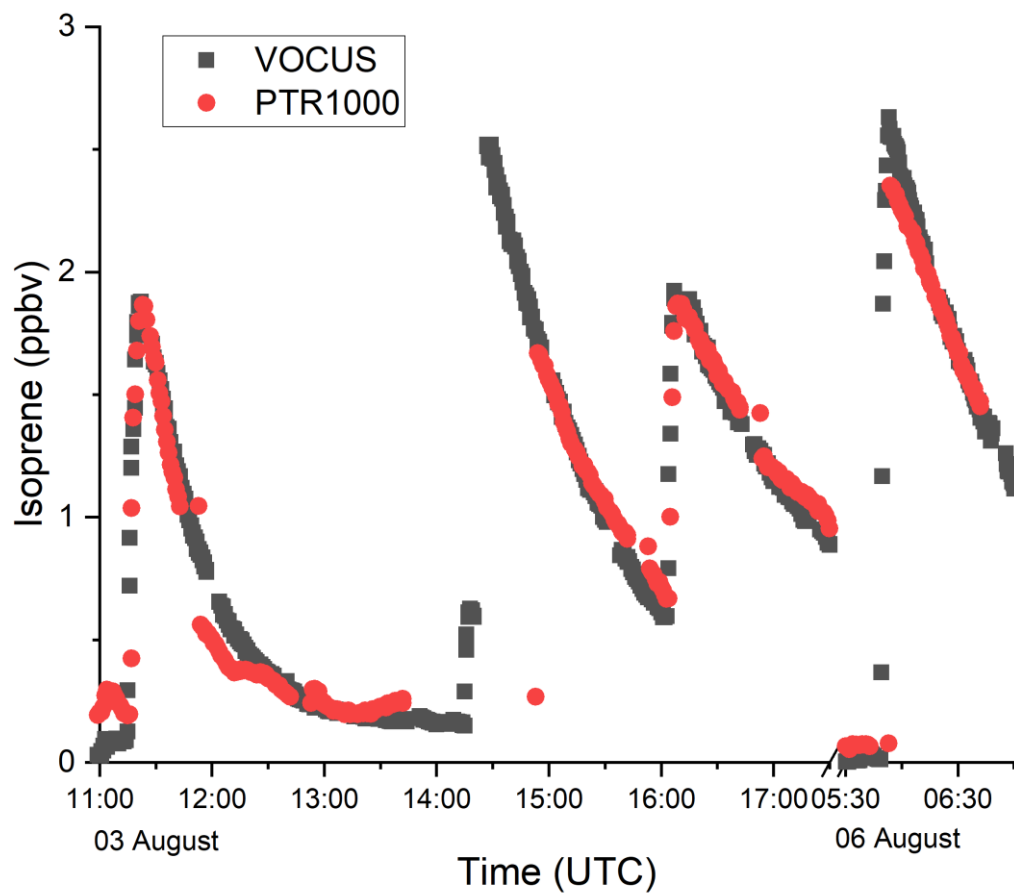


Figure S1: Amounts of isoprene during parts of the experiments on the 3rd and 6th August as measured by the two available PTR-ToF-MS instruments Vocus (black) and PTR1000 (red).

55 Comparison of k^{OH} and k^{NO_3}

During NO3ISOP, k^{OH} was measured with an instrument based on laser photolysis – laser induced fluorescence (LP-LIF) (Hofzumahaus et al., 2009; Lou et al., 2010; Fuchs et al., 2017a; Fuchs et al., 2017b). Ambient air was passed at a flow rate of 19 L min⁻¹ through a flow tube and part of the air was drawn into an OH fluorescence detection cell. OH radicals were produced within a few nanoseconds in the flow tube by pulsed laser-photolysis of O₃ (at 266 nm) with subsequent reaction of O(¹D) atoms with water vapour. OH concentration profiles were recorded by LIF, with k^{OH} determined from the exponential decay constant after correction for diffusion / wall loss (1.8 ± 0.15 s⁻¹). The time resolution of the k^{OH} measurements was 90 s with a limit of detection of 0.5 s⁻¹. The resulting accuracy of k^{OH} is (5-10) % ± 0.2 s⁻¹ at NO mixing ratios below 20 ppbv. Each isoprene injection results in an increase in reactivity of both OH and NO₃. Within the first few minutes after an isoprene injection, the contribution of secondary oxidation products to both k^{NO_3} and k^{OH} is negligible. Hence, the increase in the OH- and NO₃ reactivity (Δk^{OH} and Δk^{NO_3}) directly after an isoprene injection scales with the amount of isoprene injected and the corresponding rate coefficient ($k_{NO_3+C_5H_8} = 6.5 \times 10^{-13}$ cm³ molecule⁻¹ s⁻¹, $k_{OH+C_5H_8} = 1 \times 10^{-10}$ cm³ molecule⁻¹ s⁻¹ at 298 K (IUPAC, 2019)). For any particular injection, both approaches should lead to similar isoprene concentrations as shown in Eq. S1.

$$[\text{Isoprene}] = \frac{\Delta k^{OH}}{k_{OH+C_5H_8}} = \frac{\Delta k^{NO_3}}{k_{NO_3+C_5H_8}} \quad (\text{S1})$$

Figure S2 plots the isoprene mixing ratios derived from measurements of Δk^{OH} versus those derived from Δk^{NO_3} . For experiments with isoprene mixing ratios below ~5 ppbv a slope of 0.88 ± 0.11 was obtained. During two injections, when high concentrations of isoprene (~11 and ~22 ppbv) were injected in the chamber, the Δk^{OH} measurement returns isoprene mixing ratios that are significantly lower than those derived from Δk^{NO_3} and the mixing ratio expected from the amount of isoprene injected. On these days, a combination of the low laser power and a small number of points to fit the (rapid) exponential decay mean that the OH reactivity must be considered a lower-limit.

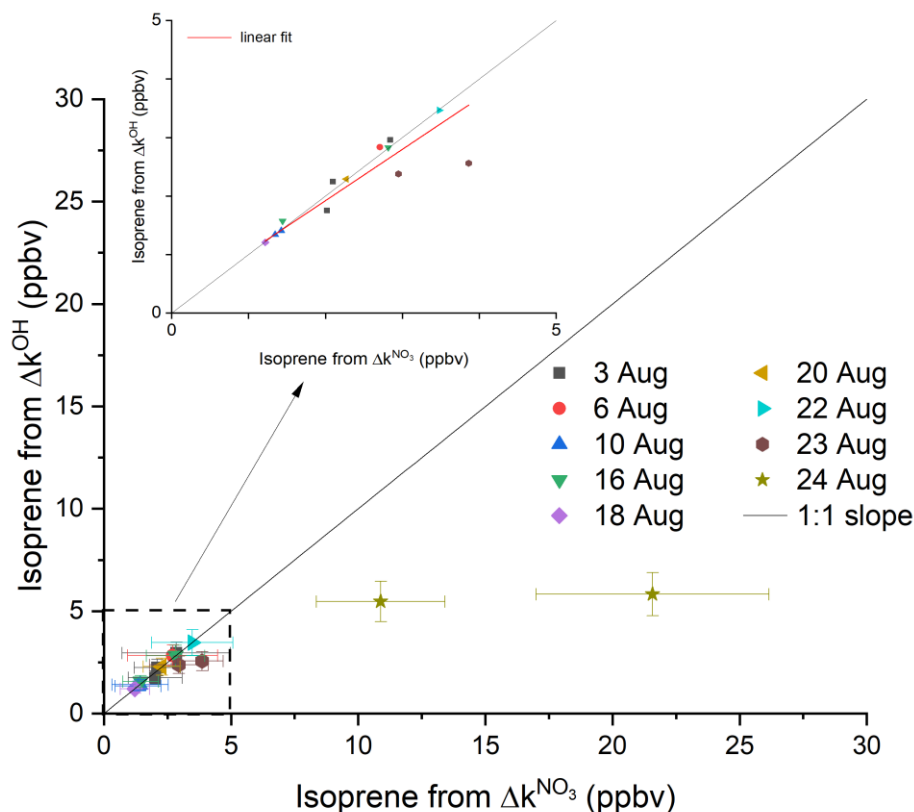
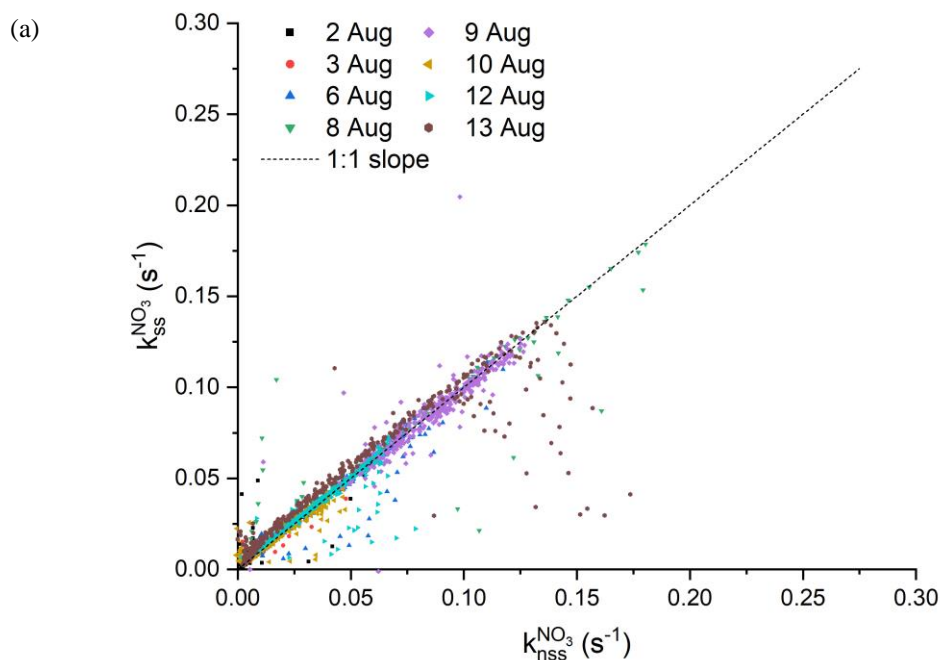


Figure S2: Isoprene mixing ratios deduced from Δk^{OH} against those from Δk^{NO_3} under the usage of Eq. (S1) for isoprene injections of different experiments (days). The error bars denote the associated uncertainties in Δk^{NO_3} (4-70%, Liebmann et al., 2017) and $k_{NO_3+C_5H_8}$ (41% (IUPAC, 2019)) and Δk^{OH} (10%, for [isoprene] < 5 ppbv) and $k_{OH+C_5H_8}$ (15% (IUPAC, 2019)). The black line indicates the case of ideal 1:1 correlation, the red line shows an orthogonal linear regression (slope: 0.88 ± 0.11 , intercept: 0.17 ± 0.23) for data points < 5 ppbv.

Validity of the steady-state assumption

- 85 The validity of the steady-state assumption was checked with the help of a correlation plot between the steady-state ($k_{ss}^{NO_3}$) and non-steady-state ($k_{nss}^{NO_3}$) reactivity as depicted in Fig. S3a. A slope close to 1 is found for most of the experiments. At injection points of NO_2 or at low reactivities larger differences are observed which are related to short-term perturbation of the equilibrium between NO_3 and N_2O_5 and deviation from steady-state.
- 90 Figure S3b compares $k_{ss}^{NO_3}$ with $k_{nss}^{NO_3}$ on the 2nd August. Between 9:00 and 11:00 UTC only NO_2 and O_3 were injected into chamber so that the influence of the chamber alone (reaction with the walls and the dilution flow) determines the NO_3 losses. As the NO_3 loss rate is low under these circumstances, nearly half an hour is necessary to achieve steady-state. This is confirmed by the difference between $k_{nss}^{NO_3}$ and $k_{ss}^{NO_3}$. Under the experimental conditions, the equilibrium between NO_3 and N_2O_5 is reached more rapidly than the steady state (Brown et al., 2003). Consequently, $k_{nss}^{NO_3}$ acquires a constant value earlier
- 95 than $k_{ss}^{NO_3}$. A reinjection of NO_2 at ~10:50 perturbs the stationary-state and therefore strongly affects $k_{ss}^{NO_3}$ whereas $k_{nss}^{NO_3}$ remains mostly unchanged. After the injection of isoprene the high NO_3 -reactivity means that the steady-state assumption becomes valid, which leads to an agreement between the two methods.



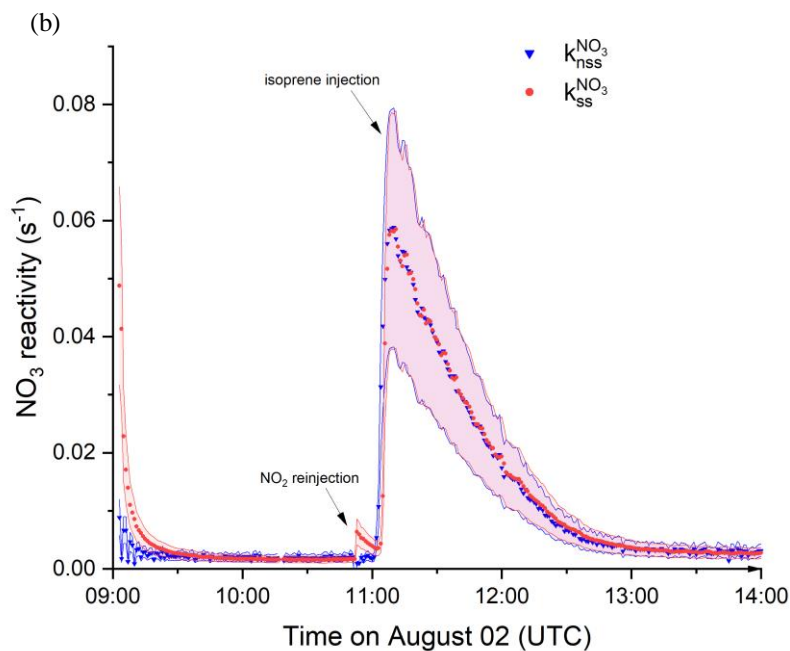


Figure S3: (a) Steady-state $k_{ss}^{NO_3}$ and non-steady-state $k_{nss}^{NO_3}$ reactivities sorted by experiment. The dotted line through the origin with a slope of 1 represents perfect agreement. (b) Comparison between steady- (red) and non-steady-state (blue) reactivities on the experiment of the 2nd August. The respective uncertainties obtained from error propagation of the uncertainties in k_2 (15%; IUPAC, 2019) and the NO_3 , NO_2 and O_3 mixing ratios (25%, 9% and 5%, respectively) are indicated by areas in the same colour of the data points.

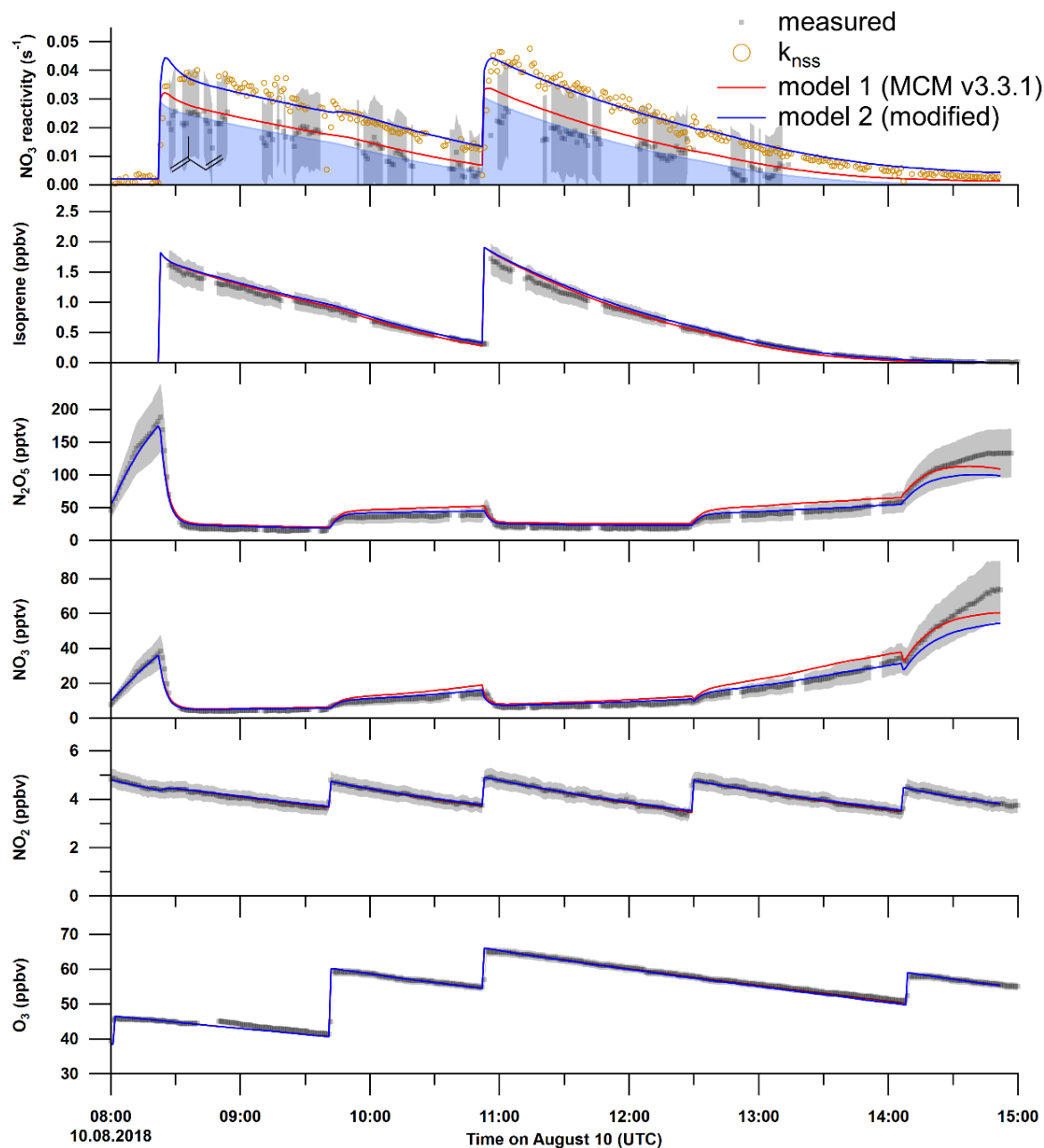


Figure S4: O₃, NO₂, NO₃, N₂O₅ and isoprene mixing ratios as well as the NO₃ reactivity on the experiment of the 10th August (black). The grey shaded area symbolizes the overall uncertainty associated with each measurement. Orange circles denote the non-steady-state reactivity obtained from Eq.(3). The results of the numerical simulation using MCM v.3.3.1 (with NO₃ and N₂O₅ wall loss rate of 0.016 s⁻¹ and 3.3 × 10⁻⁴ s⁻¹ respectively) for each of the reactants is shown by a red line, whereas the blue line shows the result of the same model with a doubled reaction constant for NO₃ + RO₂ reactions ($k_{NO_3+RO_2} = 9.2 \times 10^{-12} \text{ cm}^3 \text{ molecule}^{-1} \text{ s}^{-1}$).

References

- 115 Brown, S. S., Stark, H., and Ravishankara, A. R.: Applicability of the steady state approximation to the interpretation of atmospheric observations of NO₃ and N₂O₅, *J. Geophys. Res. -Atmos.*, 108, Art. 4539, doi:10.1029/2003JD003407, 2003.
Fuchs, H., Hofzumahaus, A., Rohrer, F., Bohn, B., Brauers, T., Dorn, H. P., Haseler, R., Holland, F., Kaminski, M., Li, X., Lu, K., Nehr, S., Tillmann, R., Wegener, R., and Wahner, A.: Experimental evidence for efficient hydroxyl radical regeneration in isoprene oxidation, *Nat. Geosci.*, 6, 1023-1026, doi:10.1038/Ngeo1964, 2013.
- 120 Fuchs, H., Novelli, A., Rolletter, M., Hofzumahaus, A., Pfannerstill, E. Y., Kessel, S., Edtbauer, A., Williams, J., Michoud, V., Dusanter, S., Locoge, N., Zannoni, N., Gros, V., Truong, F., Sarda-Esteve, R., Cryer, D. R., Brumby, C. A., Whalley, L. K., Stone, D., Seakins, P. W., Heard, D. E., Schoemaeker, C., Blocquet, M., Coudert, S., Batut, S., Fittschen, C., Thames, A. B., Brune, W. H., Ernest, C., Harder, H., Muller, J. B. A., Elste, T., Kubistin, D., Andres, S., Bohn, B., Hohaus, T., Holland, F., Li, X., Rohrer, F., Kiendler-Scharr, A., Tillmann, R., Wegener, R., Yu, Z. J., Zou, Q., and Wahner, A.: Comparison of OH reactivity measurements in the atmospheric simulation chamber SAPHIR, *Atmos. Meas. Tech.*, 10, 4023-4053, doi:10.5194/amt-10-4023-2017, 2017a.
Fuchs, H., Tan, Z. F., Lu, K. D., Bohn, B., Broch, S., Brown, S. S., Dong, H. B., Gomm, S., Haseler, R., He, L. Y., Hofzumahaus, A., Holland, F., Li, X., Liu, Y., Lu, S. H., Min, K. E., Rohrer, F., Shao, M., Wang, B. L., Wang, M., Wu, Y. S., Zeng, L. M., Zhang, Y. S., Wahner, A., and Zhang, Y. H.: OH reactivity at a rural site (Wangdu) in the North China Plain: contributions from OH reactants and experimental OH budget, *Atmos. Chem. Phys.*, 17, 645-661, doi:10.5194/acp-17-645-2017, 2017b.
- 130 Hjorth, J., Ottobriani, G., and Restelli, G.: Reaction of the NO₃ radical with CO: Determination of an upper limit for the rate constant using FTIR spectroscopy, *Int. J. Chem. Kinet.*, 18, 819-827, doi:10.1002/kin.550180802, 1986.
Hofzumahaus, A., Rohrer, F., Lu, K. D., Bohn, B., Brauers, T., Chang, C. C., Fuchs, H., Holland, F., Kita, K., Kondo, Y., Li, X., Lou, S. R., Shao, M., Zeng, L. M., Wahner, A., and Zhang, Y. H.: Amplified Trace Gas Removal in the Troposphere, *Science*, 324, 1702-1704, 2009.
IUPAC: Task Group on Atmospheric Chemical Kinetic Data Evaluation, (Ammann, M., Cox, R.A., Crowley, J.N., Herrmann, H., Jenkin, M.E., McNeill, V.F., Mellouki, A., Rossi, M. J., Troe, J. and Wallington, T. J.) <http://iupac.pole-ether.fr/index.html>, 2019.
- 135 Jenkin, M. E., Wyche, K. P., Evans, C. J., Carr, T., Monks, P. S., Alfarra, M. R., Barley, M. H., McFiggans, G. B., Young, J. C., and Rickard, A. R.: Development and chamber evaluation of the MCM v3.2 degradation scheme for beta-caryophyllene, *Atmos. Chem. Phys.*, 12, 5275-5308, doi:10.5194/acp-12-5275-2012, 2012.
- 140 Jenkin, M. E., Young, J. C., and Rickard, A. R.: The MCM v3.3.1 degradation scheme for isoprene, *Atmos. Chem. Phys.*, 15, 11433-11459, doi:10.5194/acp-15-11433-2015, 2015.
Lou, S., Holland, F., Rohrer, F., Lu, K., Bohn, B., Brauers, T., Chang, C. C., Fuchs, H., Haseler, R., Kita, K., Kondo, Y., Li, X., Shao, M., Zeng, L., Wahner, A., Zhang, Y., Wang, W., and Hofzumahaus, A.: Atmospheric OH reactivities in the Pearl River Delta - China in summer 2006: measurement and model results, *Atmos. Chem. Phys.*, 10, 11243-11260, doi:10.5194/acp-10-11243-2010, 2010.
- 145 Richter, C.A.: Ozone Production in the Atmosphere Simulation Chamber SAPHIR, Ph.D. thesis, Forschungszentrum Jülich GmbH, University of Köln, http://user.fz-juelich.de/record/62596/files/Energie&Umwelt_02.pdf, 2007.